THE UNIVERSITY OF
ARIZONA
TUCSON ARIZONA

THERMAL CONTROL SYSTEMS FOR LOW-TEMPERATURE HEAT REJECTION ON A LUNAR BASE

K. R. Sridhar
Principal Investigator

and

Matthias Gottmann
Graduate Research Assistant

Progress Report
for

Grant NAG5-1572
from
NASA Goddard Space Flight Center

Aerospace and Mechanical Engineering
The University of Arizona

October 1992

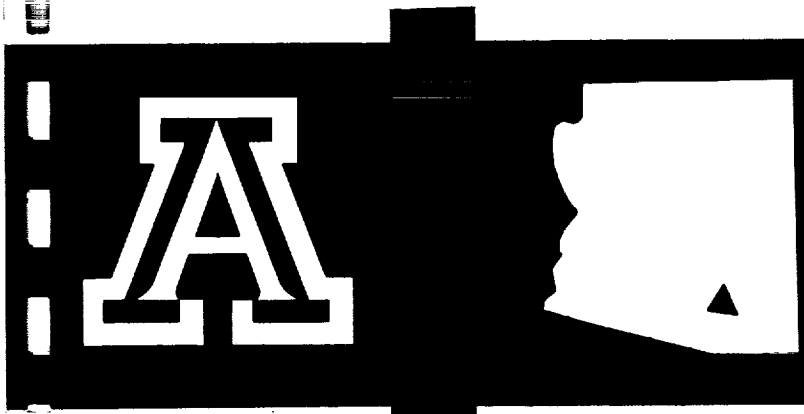

ENGINEERING EXPERIMENT STATION
COLLEGE OF ENGINEERING AND MINES
THE UNIVERSITY OF ARIZONA
TUCSON, ARIZONA 85721

THERMAL CONTROL SYSTEMS FOR LOW-TEMPERATURE HEAT REJECTION ON A LUNAR BASE

K. R. Sridhar
Principal Investigator

and

Matthias Gottmann
Graduate Research Assistant

Final Report
for
Grant NAG5-1572
from
NASA Goddard Space Flight Center

Aerospace and Mechanical Engineering
The University of Arizona
October 1992

EXECUTIVE SUMMARY

One of the important issues in the design of a lunar base is the thermal control system (TCS) used to reject low-temperature heat from the base. The TCS ensures that the base and the components inside are maintained within an acceptable temperature range. The temperature of the lunar surface peaks at 400 K during the 336-hour lunar day. Under these circumstances, direct dissipation of waste heat from the lunar base using passive radiators would be impractical. Thermal control systems based on thermal storage, shaded radiators, and heat pumps have been proposed. Based on proven technology, innovation, realistic complexity, reliability, and near-term applicability, a heat pump-based TCS was selected as a candidate for early missions.

In this report, Rankine-cycle heat pumps and absorption heat pumps (ammonia-water and lithium bromide-water) have been analyzed and optimized for a lunar base cooling load of 100 kW. For the Rankine cycle, a search of several commonly used commercial refrigerants provided R11 and R717 as possible working fluids. Hence, the Rankine-cycle analysis has been performed for both R11 and R717. Two different configurations were considered for the system--one in which the heat pump is directly connected to the rejection loop and another in which a heat exchanger connects the heat pump to the rejection loop. For a marginal increase in mass, the decoupling of the rejection loop and the radiator from the heat pump provides greater reliability of the system and better control. Hence, the decoupled system is the configuration of choice. The optimal TCS mass for a 100 kW cooling load at 270 K was 5940 kg at a radiator temperature of 362 K. R11 was the working fluid in the heat pump, and R717 was the transport fluid in the rejection loop.

Two TCSs based on an absorption-cycle heat pump were considered, one with an ammonia-water mixture and the other with a lithium bromide-water mixture as the working fluid. A complete cycle analysis was performed for these systems. The system components were approximated as heat exchangers with no internal pressure

drop for the mass estimate. This simple approach underpredicts the mass of the systems, but is a good "optimistic" first approximation to the TCS mass in the absence of reliable component mass data. The mass estimates of the two systems reveal that, in spite of this optimistic estimate, the absorption heat pumps are not competitive with the Rankine-cycle heat pumps.

Future work at the systems level will involve similar analyses for the Brayton- and Stirling-cycle heat pumps. The analyses will also consider the operation of the pump under partial-load conditions. On the component level, a capillary evaporator will be designed, built, and tested in order to investigate its suitability in lunar base TCS and microgravity two-phase applications.

TABLE OF CONTENTS

LIST OF TABLES

LIST OF FIGURES

LIST OF FIGURES (continued)

CHAPTER 1. INTRODUCTION

One of the important issues in the architecture of a lunar base is the design of a thermal control system (TCS) to reject the low-temperature heat from the base. The TCS ensures that the base and all the components inside are maintained within the operating temperature range. The temperatures of the lunar surface peak to about 400 K during the 336-hour lunar day, and the issue of low-temperature (less than 400 K) heat rejection from the base under such conditions is a technically challenging one. Prior studies have shown that the overall mass of a TCS and its power supply under such circumstances can be significant [1-3].

The single largest fraction of the overall cost for any space mission is associated with the initial launch, which continues to be in the vicinity of $6,000-$12,000/kg from Earth to LEO. The reduction of lift mass at launch is a key design driver in space mission planning. In attempts to find the lowest mass for the TCS, several options have been proposed. One option would be to store the waste heat deep in the lunar regolith [1], which would require a piping system, working as a heat exchanger, to be buried in the soil. The technical difficulties and uncertainties associated with large-scale excavation on the Moon, and a lack of knowledge about the thermal properties of lunar regolith, are primary reasons for not pursuing this path at this juncture. However, this option holds promise for the future.

A significant portion of the total mass of the TCS is due to the radiator. Shading the radiator from the Sun and the hot lunar soil could significantly decrease the radiator's sink temperature and, hence, its mass. Therefore, the concept of shaded lightweight radiators has been proposed. This technology requires the shades to be built of specular surfaces. The degradation rate of radiator properties in a lunar environment is not known. At least for the initial cases, the prudent approach would be to employ systems that rely on proven technology. The concept of using a heat pump fits this bill. In this concept, energy in the form of heat, or work, is supplied to the

heat pump, which collects heat from the low-temperature source (the lunar base) and delivers it at a higher temperature to the radiator. The mass of a radiator dissipating high-temperature heat would be significantly lower than one operating without a temperature lift. A simplified block diagram of this concept is illustrated in Figure 1.

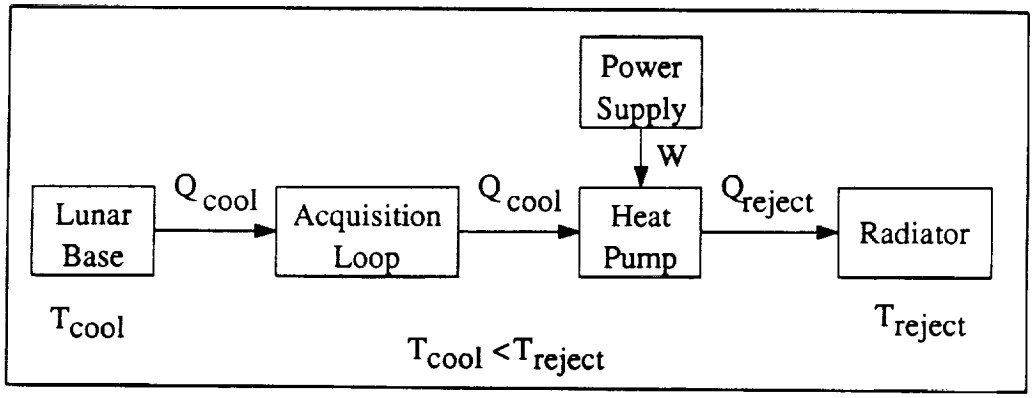

Figure 1. Schematic of a thermal control system (TCS) using a heat pump.

Heat pumps have been in use for terrestrial applications for a long time. Refrigeration devices utilizing a thermodynamic cycle are essentially heat pumps. A vapor compression cycle (involving two constant- pressure and two adiabatic processes) is the most widely used. It is also called a Rankine cycle and requires shaft work. Absorption cycles, on the other hand, are heat driven and do not require high-quality shaft work. The Stirling cycle, consisting of two isothermal and two constant-volume processes, promises a better efficiency than the Rankine cycle. Theoretically, it reaches the same efficiency as the optimal Carnot cycle, but the processes are technically difficult to realize. Today, Stirling-cycle coolers are used in cryogenic applications. Experiments using this cycle for residential heat pumps show promising results [4, 5], but these heat pumps are in their infancy in terms of their technology readiness levels.

In order to optimize the mass of the heat-pump-augmented TCS, all promising options have to be evaluated and compared. During these preliminary comparison studies, considerable care has to be given to optimizing system operating parameters,

working fluids, and component masses. However, in order to keep this preliminary study simple and concise, some issues are not being considered at this time: (1) While evaluating system mass, the control components are not accounted for since the difference in the masses for the various cycles and working fluids would not be large. (2) The systems are modeled for full-load operation, and the implications and power penalties at off-design and partial-load conditions are not considered. However, it is realized that the surface temperature of the lunar regolith varies considerably during the lunar day, as shown in Figure 2. This variation in the regolith temperature indicates that the temperature lift and the load of the heat pump vary as a function of the time of day. For this reason, the performance of the heat pump at partial-load conditions is important and will be studied in detail in the future. (3) Redundancy requirements are not considered. Issues such as these will be studied in detail during the design of the actual system. The Rankine-cycle heat pump is the first option to be studied. The details are presented in Chapter 2. Following this, the absorption cycle using both ammonia-water and lithium bromide-water mixtures are analyzed. The absorption cycle is discussed in detail in Chapter 3.

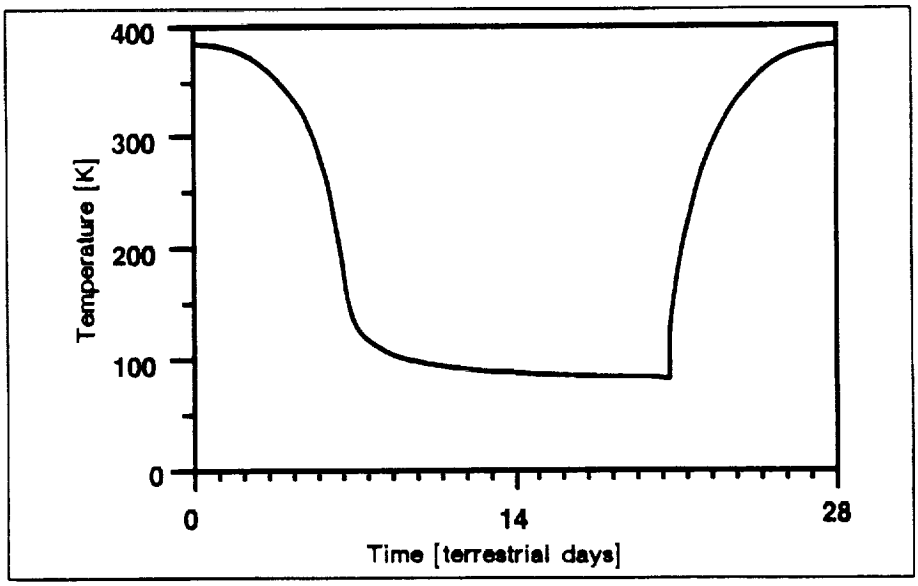

Figure 2. Variation of lunar regolith temperature with time of day.

CHAPTER 2. A THERMAL CONTROL SYSTEM BASED ON A RANKINE-CYCLE HEAT PUMP

A detailed cycle and mass analysis of a Rankine-cycle heat pump is presented in Section 2.3. Sections 2.1 and 2.2 describe the cooling load requirements for the lunar base and the design of the acquisition loop, respectively. Section 2.4 considers the mass model used for the radiator, and the mass model of the power supply is discussed in Section 2.5. The results of the mass optimization are presented in Section 2.6.

2.1 Cooling Load

In order to estimate the cooling load, a closed-system analysis was performed on a lunar base. Energies crossing the boundaries are electrical power supply, conduction through walls, and heat removed by the acquisition loop of the TCS. Internally, heat generation can occur due to human metabolic activity. The electrical power input for a first-stage base is estimated to be between 50 and 100 kW, more likely 100 kW [1, 6-8]. Conduction through the walls depends on the insulation, and it is possible to reduce heat gains or losses to a very small fraction of the electrical input without significant mass penalties. Hence, they are neglected. Based on food consumption, a crew member produces an average of about 150 W. For a crew of 6 to 8 members, the total heat generation would again be negligible, compared to the electrical input. Therefore, the cooling load (the heat removed by the acquisition loop) can be equated to the electrical input to the base. Stated differently, this implies that all electrical input will finally be dissipated as heat. The value for the cooling load is fixed at 100 kW for this study. When further details about the design and activities of the base are known, these assumptions can be revisited and refined if necessary.

2.2 The Acquisition Loop

The acquisition loop collects the excess heat from the lunar base and transports it to the heat pump. It consists of cold plates and a network of connecting pipes. The

heat is transported by a single-phase fluid. Since the coolant in the acquisition loop circulates in the habitation module, nontoxicity is a necessity for safety considerations. Water, with certain trace additives to depress its freezing point, would be a good candidate. For this study, it was decided that one cooling loop operating at a single pre-designed temperature would be used. This temperature was chosen to be 275 K (the lower of the two Space Station cooling-loop temperatures). The variation in the temperature of the coolant has to be small enough to provide isothermal cooling for small variations in the load, yet large enough to keep the coolant flow rate within reasonable limits. The mass flow rate in the acquisition loop is $\dot{m} = \dot{Q}_{cool}/(c_p \Delta T)$. If water with trace additives were used as the coolant, the temperature variation in the acquisition loop taken to be 5 K, and the water temperature to be 275 K, then the mass flow rate in the acquisition loop would be 4.8 kg/s.

2.3 The Heat Pump

Two different heat pump configurations were investigated. In the first configuration, Case A, the heat pump is directly connected to the rejection loop. In this case, the condenser of the heat pump and the radiator are one and the same. The refrigerant circulating in the heat pump condenses and rejects heat through the radiator. In the alternative configuration, Case B, the heat pump and the rejection loop are decoupled with a heat exchanger. Here, the heat exchanger is the condenser for the heat pump and a rejection loop transports the heat of condensation to the radiator for dissipation. Both the cases will be analyzed in detail in the following sections of this chapter, and their pros and cons will be discussed.

2.3.1 Heat Pump Coupled Directly to the Rejection Loop (Case A)

A simplified schematic of a heat pump directly connected to the rejection loop is illustrated in Figure 3. The main parameters of interest in the design of a heat pump used for cooling are the input heat flux ($\dot{Q}_{cool}$) and its temperature (T_{cool}), the

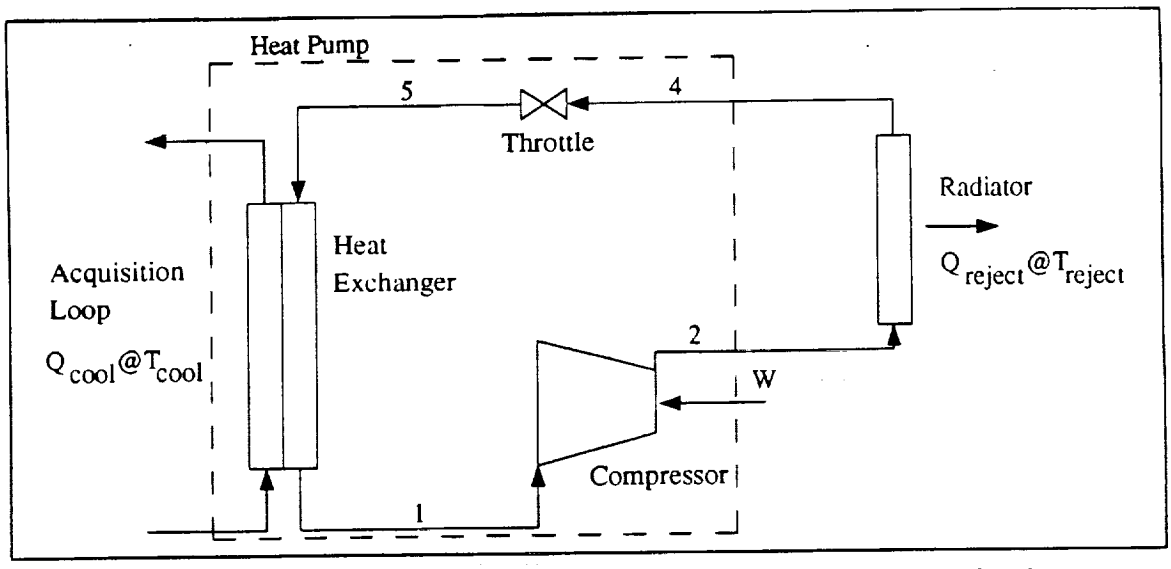

Figure 3. Schematic of a heat pump directly connected to the rejection loop.

temperature lift, and the coefficient of performance. The COP of a heat pump is defined as

$$COP = \frac{\dot{Q}_{cool}}{W_c},$$

where W_c is the power consumed by the heat pump.

The Compressor.--Figure 4 illustrates the Rankine-cycle on a p-h diagram. The working fluid in the vapor state is compressed from p_1 to p_2. Ideally, this process would be isentropic (1-2s). Due to irreversibilities, the process is nonisentropic,

$$w_{c,ideal} = h_{2s} - h_1$$

$$w_{c,\,real} = h_2 - h_1$$

$$\eta_{compressor} = \frac{h_{2s} - h_1}{h_2 - h_1},$$

where h is the specific enthalpy and the subscripts refer to the states in Figure 4.

In order to limit the number of free parameters, it is assumed that the compression would be performed in a single stage. Customarily, airplane cooling systems utilize

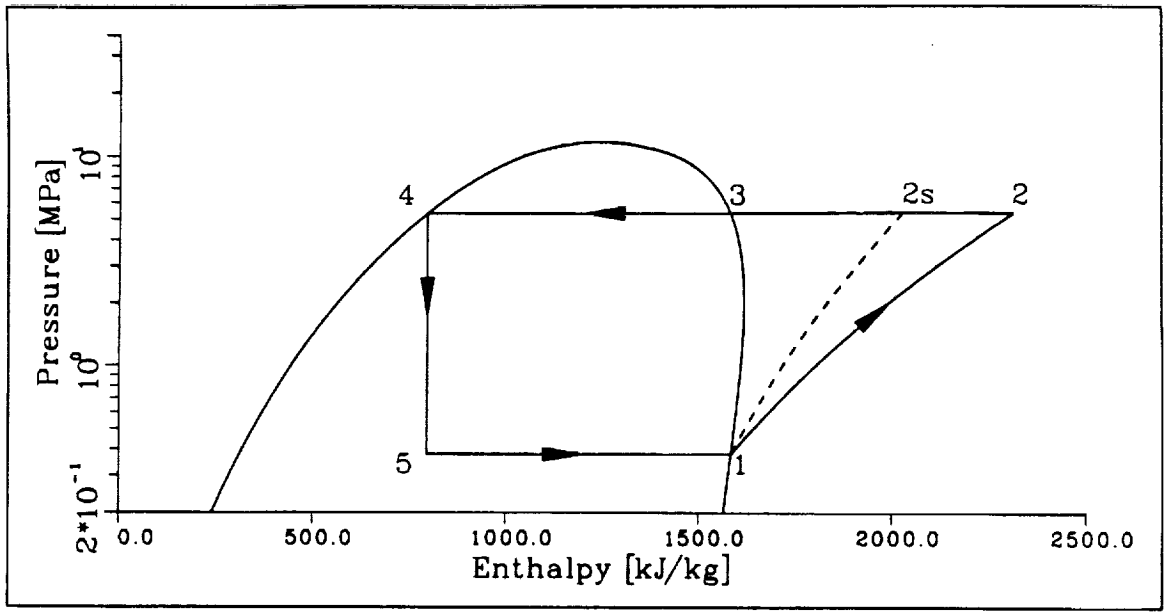

Figure 4. Rankine cycle for R717 plotted on a p-h diagram.

multistage compression [9], but there is no intercooling between the stages. Hence, effectively, the compression can be modeled to be single stage. The properties of the refrigerant used for the calculations were obtained from Reynolds [10] and a FORTRAN77 code was developed in-house [11]. Deviations from the ideal behavior in the compression occur due to mechanical, electrical (motor), and electronic (controller) inefficiencies and fluid friction. The values for the inefficiencies in state-of-the-art aircraft cooling equipment were obtained from R. Murray (AiResearch, Los Angeles, California, private communication, 1991) and are as follows: η_{mech} = 0.95, $\eta_{electrical}$ = 0.94, $\eta_{electronic}$ = 0.91, and η_{fluid} = 0.75. The excess energy supplied to overcome these inefficiencies will be converted to heat. Since the compressor would operate in a high-vacuum environment, radiation to the environment and convection of the heat by the vapor flow inside are the only heat rejection mechanisms. The contribution due to heat radiation can be shown to be negligible by modeling the compressor as a black cube, 0.25 m per side, at 400 K. Therefore, it can be assumed that all the energy supplied to the compressor will be used to compress and heat the refrigerant. The overall efficiency of the compressor is the product of all four efficiencies (61%). It

should be noted that the temperature of the compressor can be maintained within operating limits by use of a cold plate. This is not required, however, because the working fluid can convectively remove the excess heat from the compressor.

The next step is a mass estimate for the compressor. In aircraft cooling, the compressor mass is assumed to be proportional to the cooling load. One pound (0.454 kg) per kilowatt is the value suggested (R. Murray, AiResearch). In our analysis, the cooling load of the lunar base is kept a constant. The heat pump output temperature, and hence the total heat rejected by the heat pump, is varied. Since the assumption of compressor mass being proportional to the cooling load would lead to an unrealistic constant mass estimate in our case, it was modified as follows: A proportionality was assumed between compressor mass and the heat pump output, which is the sum of the input heat and compressor power. The proportionality constant was arrived at as follows: The reference temperatures to obtain the proportionality factor, T_{high} = 380 K and T_{low} = 275 K, are values typical for an aircraft cooling system. For these temperatures and R717 as the refrigerant, the heat pump overall COP is 0.805. With this value,

$$m_{comp} = \frac{M_{comp}}{\dot{Q}_{reject}} = [\dot{Q}_{cool} m'_{comp}] \left[\frac{COP}{\dot{Q}_{cool}(COP + 1)} \right] = 0.202 \text{ kg/kW} ,$$

where m_{comp} is the compressor mass in kilograms per kilowatt of rejected heat, M_{comp} is the actual compressor mass in kilograms, and m'_{comp} is the compressor mass in kilograms per kilowatt of cooling load.

Discharge and Return Lines To and From the Radiator.--At point 2 in Figure 4, the refrigerant is in the superheated state. The length of the discharge line depends on the layout of the lunar base and how the radiators are configured spatially. The discharge line has to connect all the radiators to the compressor. Figure 5 schematically depicts the setup of the radiators and the piping. Assuming the radiators

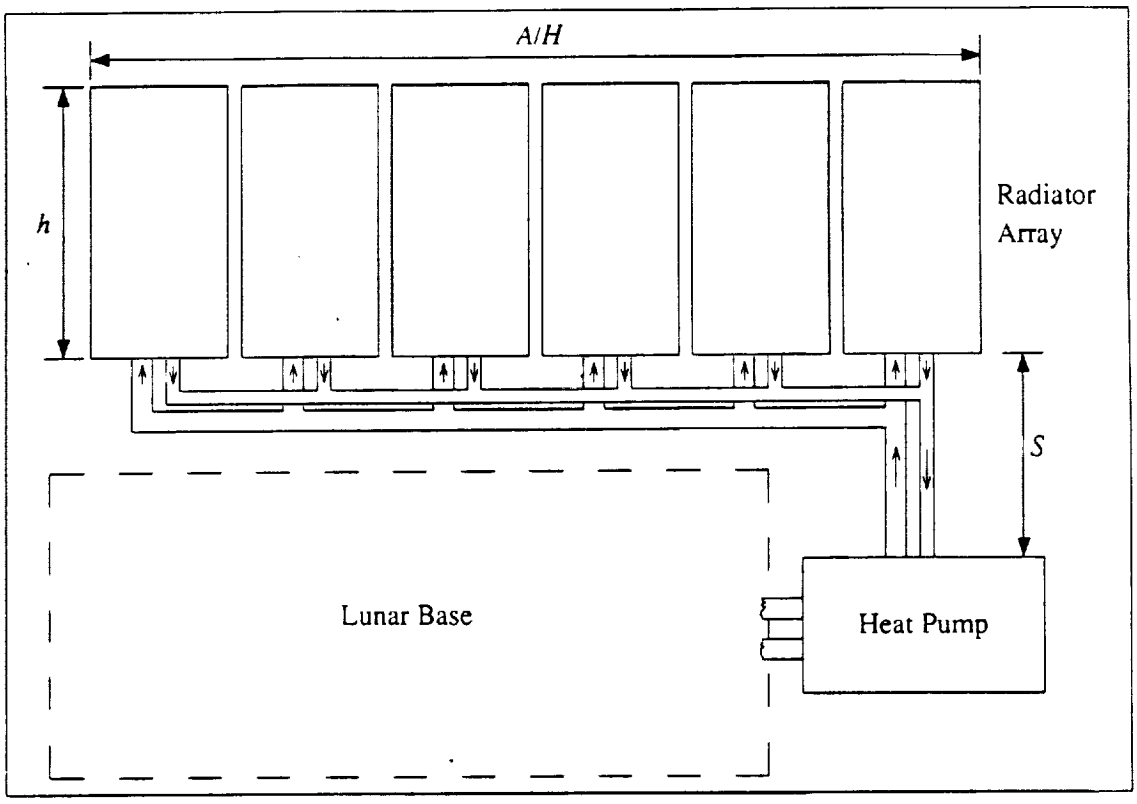

Figure 5. Schematic of radiators and rejection loop piping.

are of constant height, it is reasonable to take the pipe length to be proportional to the radiator area, i.e., L = S + A/H, where L is the length that will be used to determine the pressure drop, A is the radiator area, H is the "equivalent height" of the radiator, and S is the distance from the lunar base to the radiator array. (The equivalent height" is not the same as the actual height because it accounts for bends in the piping and/or a spacing between the radiators.) The complete rejection loop length is 2 L. The pressure drop in the piping is a function of the pipe diameter and is determined based on recommendations for good design practice [12]. The pressure drop in the discharge line, the radiator (condenser), and the return line is taken to be the equivalent of a 1 K temperature drop. It is important for the thermodynamic model that this pressure drop be small enough that it does not affect the overall efficiency. Fixing the total pressure drop allows the designer to decouple the pipe sizing from the thermodynamic evaluation of the heat pump. The pressure drop is split, such that one-half of it occurs in the condenser and the rest is in the discharge and return lines. The

friction losses in discharge and return lines are determined based on the optimization of the pipe masses. The frictional pressure drop, $(\Delta p)_f = f\ell v^2/2\rho d$, where the friction factor for smooth pipes is $f = [2 \log_{10}(2.51/Re\sqrt{f})]^{-2}$, d is the pipe diameter, ℓ is the length of the pipe, v is the fluid velocity, ρ is the fluid density, and Re is the pipe Reynolds number. The total mass is the sum of the mass of the pipe and the mass of the fluid in the pipe. The tube thickness is computed based on a factor of safety of three. A minimum thickness of 0.5 mm is also required. The density of the piping material is based on a light-weight, high-strength aluminum alloy. Should such an alloy be chemically incompatible with the refrigerant of choice, the inside of the pipes can be coated to take care of the problem. The masses are

$$M_{pipe} = \frac{\pi d^2 \ell \rho_{pipe} p}{2\sigma_{y,pipe}}$$

$$M_{fluid} = \frac{\pi d^2 \ell \rho_{fluid}}{4} ,$$

where $\sigma_{y,pipe}$ is the allowable (design) stress for the pipe material.

Between points 2 and 3, the superheated vapor is cooled in the radiator. Ideally, this process can be modeled as an isobaric process, but due to pipe friction and heat losses, a small pressure drop would occur. Between points 3 and 4, the refrigerant is condensed to saturated liquid. A finite pressure drop occurs in the condenser. The mass estimate for the condenser will be discussed in the radiator section (§2.4). The heat to be rejected by the radiator is $\dot{Q}_{reject} = h_2 - h_4$. From point 4, the saturated liquid is sent from the radiator to the throttle valve located at the evaporator inlet, through the return line. The sizing of the return line is based on the same guidelines described for the discharge line.

Evaporator and Throttle Valve.—Between points 4 and 5, the fluid is adiabatically throttled. The mass of the throttle valve is negligible compared to the mass of the other components of the heat pump. Between points 5 and 1, the refrigerant absorbs

heat from the primary coolant circulating in the lunar base. The heat removed is $\dot{Q}_{cool} = h_1 - h_5$. The mass of the evaporator is obtained based on a suggested value of 2.72 kg/kW [13].

Refrigerant.—One of the important issues is the choice of refrigerant to use as the working medium for the Rankine cycle. The refrigerants that are commonly used in terrestrial and aerospace applications, R11, R12, R113, R114, and R717, were considered [9]. R113 and R114 were eliminated from the list of potential refrigerants because of the possibility of condensation of the vapor in the compressor (Figure 6). Such condensation would be detrimental to the life of the compressor. The selection was then narrowed to R11 and R717, because R12 has a lower COP and a lower critical temperature (R717: T_{crit} = 407 K; R11: T_{crit} = 474 k; R12 : T_{crit} = 385 K). The p-h diagrams for R717 and R11 are shown in Figures 4 and 7, respectively. Safety considerations give an edge to R11 because of its nontoxicity and noninflammability, but R717 offers better heat transport properties. The thermodynamic properties of the refrigerants were obtained using the analytical functions suggested by Reynolds [10]. The COP can be expressed in terms of the specific enthalpies as

$$COP = \frac{h_2 - h_5}{h_2 - h_1} .$$

The overall COP was computed as a function of the condenser temperature and is plotted in Figure 8. Table 1 lists the COP calculations for a condenser temperature of 380 K.

Implementation of Heat Pump and Piping Model.—Values for COP and the mass of the piping were computed and tabulated for varying rejection temperatures using the models discussed above. These tabulated values were imported to a spreadsheet and linearly interpolated where necessary.

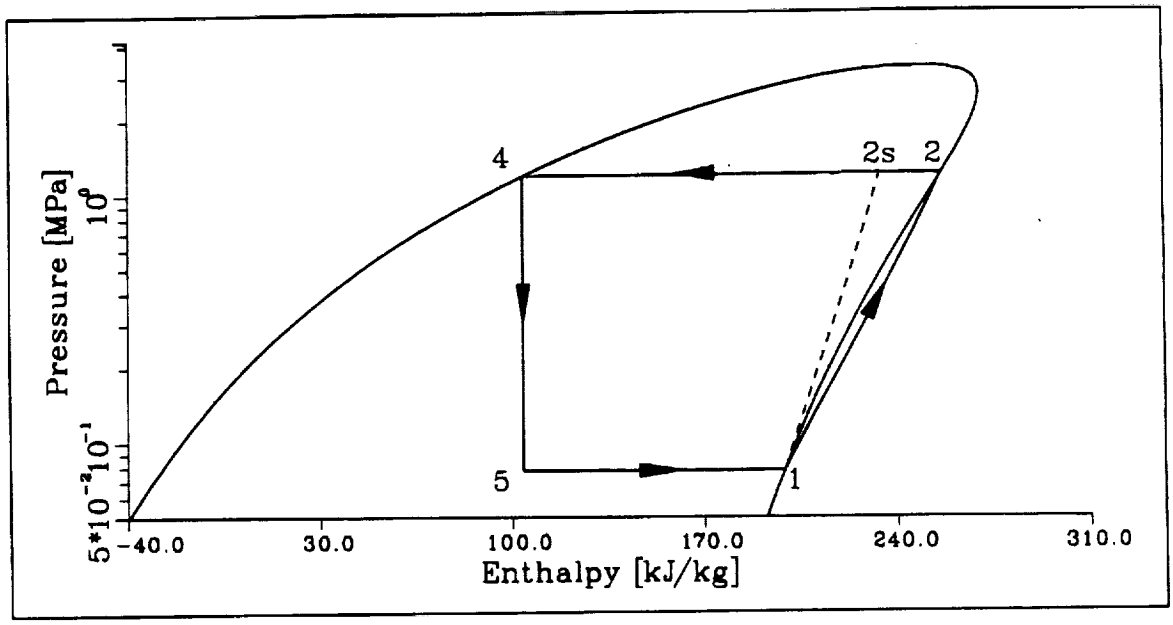

Figure 6. Rankine cycle for R114 (T_{low} = 270 K, T_{high} = 360 K).

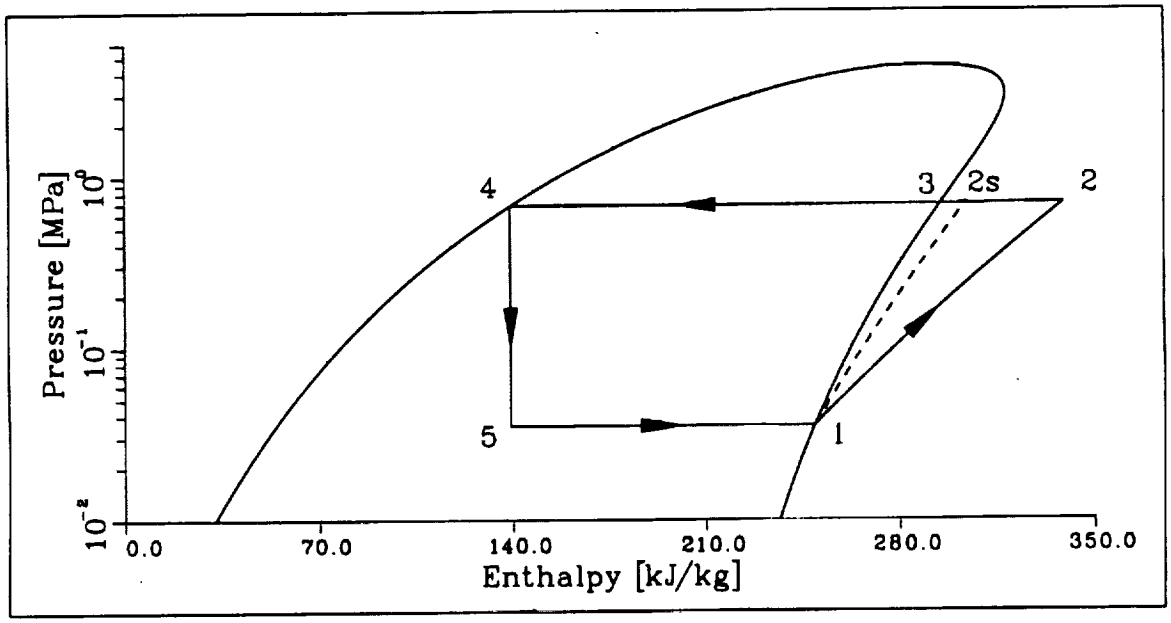

Figure 7. Rankine cycle for R11 (T_{low} = 270 K, T_{high} = 360 K).

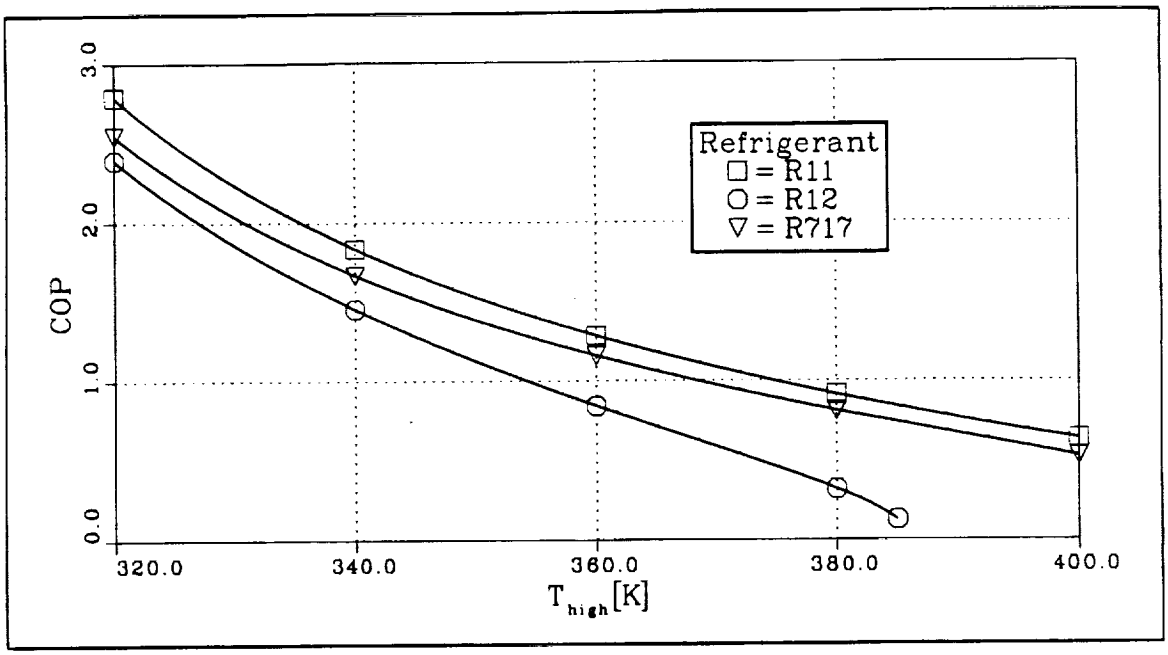

Figure 8. Variation of COP with condenser temperature for R11, R12, and R717.

Table 1. Properties of R717 and R11 in the Rankine cycle for T_{high} = 380 K.

State	T [K]	P [MPa]	h [kJ/kg]	s [kJ/kg]	ρ [kg/m^3]
R717: COP = 0.829					
1	270	0.381	1584	6.046	3.088
2	626	7.270	2419	6.615	24.890
3	380	7.140	1541	4.788	67.200
4	380	7.140	893	3.080	436.500
5	270	0.381	893	3.483	6.725
R11: COP = 0.914					
1	270	0.035	249	0.9581	2.18
2	448	0.964	350	1.0510	39.20
3	380	0.945	301	0.9343	49.70
4	380	0.945	158	0.5565	1255.00
5	270	0.035	158	0.6180	4.22

2.3.2 Heat Pump Decoupled from Rejection Loop by Heat Exchanger (Case B)

Connecting the heat pump directly to the radiator has inherent disadvantages. If the refrigerant used in the Rankine cycle is not the best one for a heat transport loop, it would be advantageous to separate the rejection loop from the heat pump using a heat exchanger. This configuration, a heat pump-augmented TCS, is shown in Figure 9. From a system-design perspective, it is desirable to decouple subsystems that carry out different tasks. The decoupled case would provide for better and simpler control of the TCS during partial-load conditions. On the other hand, a heat exchanger between the two loops would cause a temperature drop between the heat pump and the rejection loop and an associated mass penalty. To compensate for the temperature drop, the heat pump has to deliver the output heat at a higher temperature and therefore operate at a lower COP. If the same fluid were used in the Rankine cycle and in the rejection loop, the only foreseeable advantage of the decoupled system would be the possibility of better and simpler control. However, other advantages could emerge if two different fluids were used. Many heat pumps operating in parallel could share the same decoupled rejection loop. Also, a meteorite hit of the rejection loop piping would not put the heat pump out of commission.

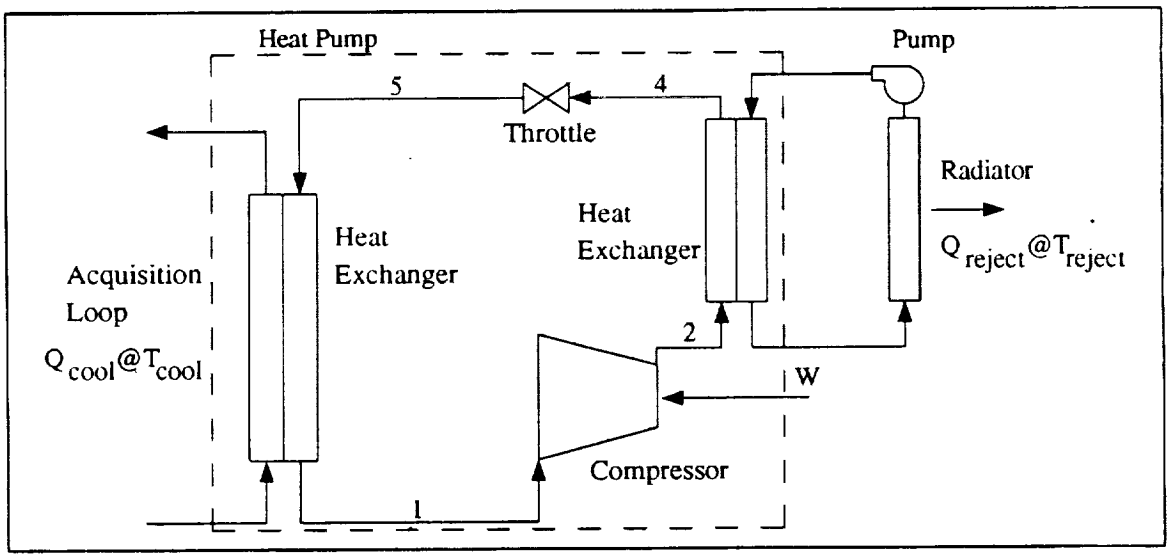

Figure 9. Schematic of a heat pump decoupled from the rejection loop.

The thermodynamic and mass models for the heat pump with an output heat exchanger (Case B) differ only in a few aspects from the models presented for Case A (§2.3.1). Only these differences will be discussed here.

Condenser.—In Case B, the condenser is a heat exchanger that decouples the rejection loop from the heat pump. Both fluids undergo phase changes in this heat exchanger. For a mass estimate, the value quoted by Swanson et al. [1], 2.72 kg/kW, was used. The thermodynamic performance of the condenser is characterized by a pressure drop in each loop (heat pump and rejection loop) and a temperature difference between both sides. The temperature difference is set to 5 K, the same as for the acquisition side. Consistent with Case A, the pressure drop has to be small enough so as not to affect the heat pump's performance. A pressure drop equivalent to a 1 K temperature drop has been assigned to the condenser.

Rankine-Cycle Analysis.—The cycle evaluation follows the same path outlined for Case A. The efficiencies and pressure drops of the heat pump components are also the same as in Case A. The COP as a function of the output temperature, T_{high}, was computed with a FORTRAN77 program using the fluid properties given by Reynolds [10]. The implementation of this COP(T) in the spreadsheet was realized with an approximate analytical function. For each refrigerant, a fourth-order polynomial was fitted to the data computed with the FORTRAN77 code. The resulting approximation yields an error of less than 0.3 percent for output temperatures from T_{high} = 320 K to T_{high} = 390 K. Figure 10 shows a comparison between the real fluid model and the polynomial approximation, and Figure 11 presents the corresponding error analysis. It can be seen that the results are almost identical.

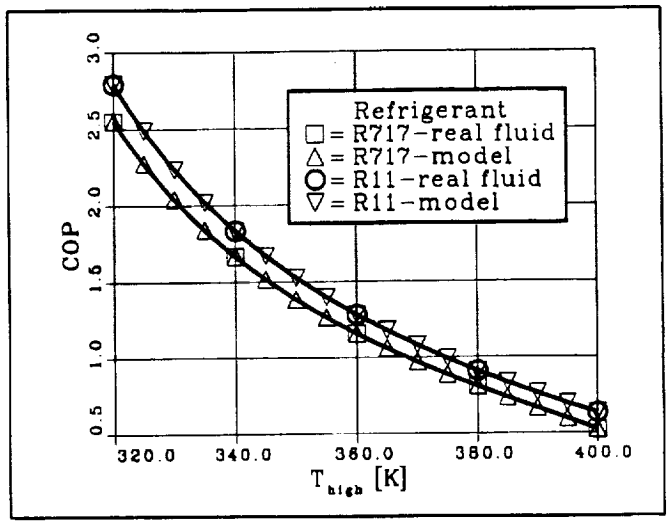

Figure 10. Comparison of COP from cycle analysis and approximation for R11 and R717 (T_{evap} = 270 K).

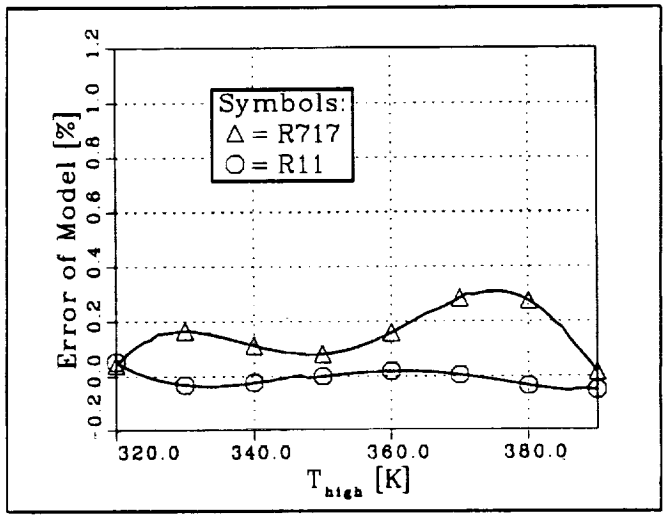

Figure 11. Error analysis for the approximation shown in Figure 10.

Rejection Loop.—The decoupled rejection loop would require a pump to circulate the coolant fluid. This pump and the power penalty associated with it have to be incorporated into the mass estimate and optimization. The pump mass is estimated using a formula quoted by Dexter and Haskin [2],

$$M_{pump} = 5.61\left[\frac{\dot{m}}{60\,\rho}\right]^{0.75},$$

where $\dot{m}$ is the mass flow rate in pounds per hour and ρ is the density of the fluid in pounds per cubic foot. The power required for a liquid pump can be readily computed from

$$W_{pump} = \frac{\Delta P \dot{V}}{\eta_{pump}},$$

where ΔP is the pressure differential across the pump, $\dot{V}$ is the volume flow rate, and η_{pump} is the pump efficiency. A conservative value, $\eta_{pump} = 0.25$, as suggested by Dexter and Haskin [2] was used. The pressure drop was determined with the formulas presented for Case A. The pipe thickness is again determined based on the hoop stress or 0.5 mm, whichever is larger. Masses included in the estimate are due to pipes, coolant, pump, and the power supply. The decoupled rejection loop does not affect the heat pump COP. The minimum mass for the loop may be achieved by balancing pipe mass and the power penalty. This approach results in optimum mass when the pipe diameters are relatively small and the pressure drop is large. However, a large pressure drop in the vapor line would result in a large temperature drop, and this is accompanied by an increase in the radiator area and mass. While the pressure drop in the liquid line can be compensated for by the pump, if the pressure drop gets large, the pumping power will become significant and add to the total heat rejection load. Therefore, the mass estimate for the piping has to be computed based on a limited pressure drop. Here, again, the pressure drop is specified in terms of an equivalent temperature drop and is set to 0.5 K in the vapor and 1.0 K in the liquid line. These values are chosen based on recommended design practice [12]. The cooling fluid of choice is ammonia, which has already demonstrated its good performance as a heat transport fluid in Case A. The toxicity of ammonia will not be a concern in the rejection loop because it is outside the habitation modules.

In Case A, the piping mass was determined with the heat pump estimate because they are coupled. Assuming values for the radiator height and distance from the base, Case A yielded a model where the piping mass depends solely on the rejection temperature. For Case B, a model that makes use of the decoupling of heat pump characteristics and the rejection loop was sought. For a given refrigerant and specified pressure drops in the liquid and vapor lines, the rejection loop mass depends on three parameters: rejection heat load, Q_{reject}; rejection temperature, T_{reject}; and pipe length, L_{reject}. Using the thermodynamic properties from Reynolds [10], the mass model was implemented in a FORTRAN77 code. Figures 12 and 13 show results obtained with the code. For use with a spreadsheet, it is desirable to obtain an analytical expression for the mass. This was realized with a polynomial that is second order in temperature, second order in height, and linear in rejection heat load:

$$M_{piping} = \sum_{i=0}^{2} \sum_{j=0}^{2} \sum_{k=0}^{1} a_{ijk} T^i L^j Q^k \ .$$

The coefficients were determined with a least square error fit. The approximation is valid in the following range: 340 K $\leq T_{reject} \leq$ 380 K, 150 kW $\leq Q_{reject} \leq$ 250 kW, and 100 m $\leq L_{reject} \leq$ 400 m. The maximum error of the approximation is 3 percent.

2.4 Radiator Considerations

The function of the radiator is to reject the waste heat from the base. The heat rejected by the radiator is given by $\dot{Q} = A\epsilon\eta\sigma(T_{reject}^4 - T_{sink})$, where ϵ is the emissivity, η is the fin efficiency, and T_{reject} and T_{sink} are the radiator and sink temperature, respectively. The estimated sink temperature for a vertically mounted radiator at the lunar base is 321 K [6]. Most reviewed sources suggest $\epsilon = 0.8$ and $\eta = 0.7$. Several estimates for the mass of a radiator are available in the literature [1-3, 6, 14-16]. The mass of a radiator is taken to be proportional to its area, and recent publications

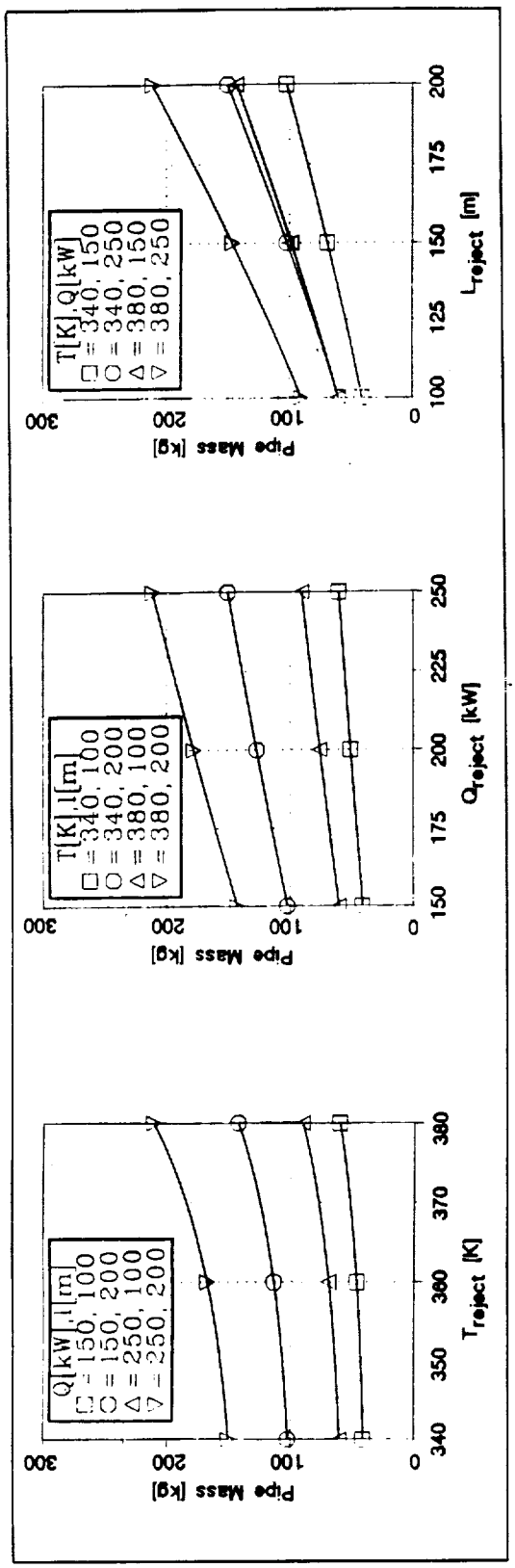

Figure 12. Mass of the rejection loop piping (liquid).

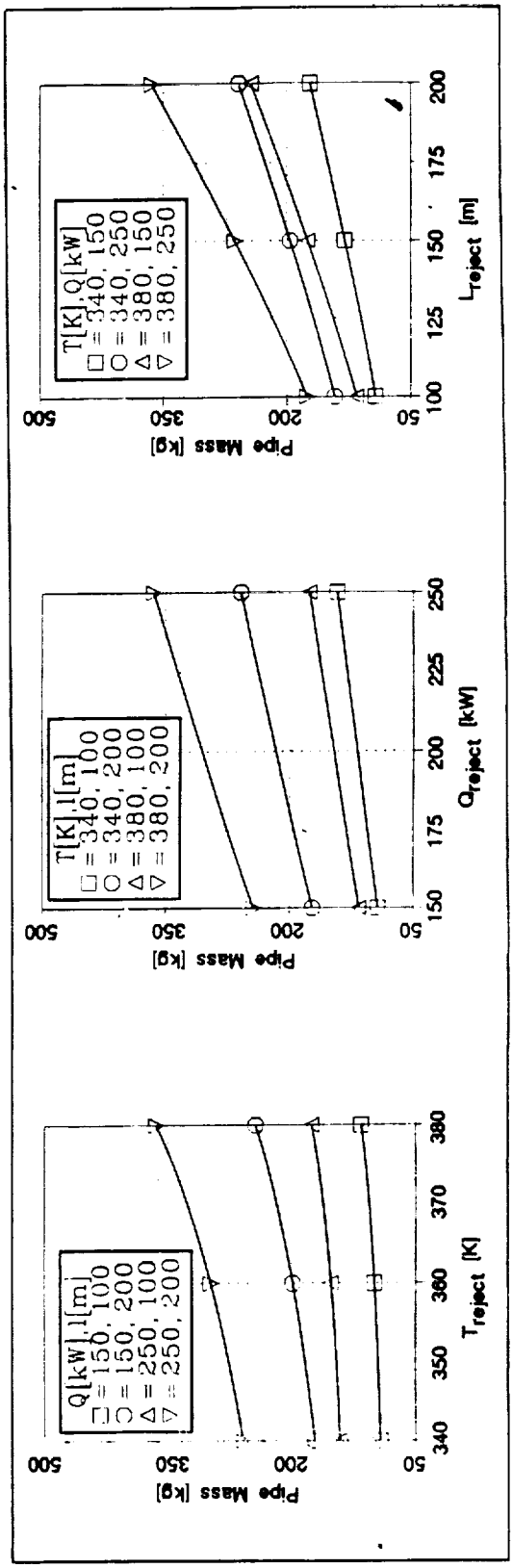

Figure 13. Mass of the rejection loop piping (vapor).

recommend a value of 5 kg/m^2 for a one-sided radiator. The vertical radiator is two sided and hence a mass estimate of 2.5 kg/m^2 is assumed. Other values of specific mass of the radiator can be incorporated in the spreadsheet without difficulty. The heat to be rejected is the cooling load of the base plus the power consumed to operate the heat pump.

2.5 Power Supply

The heat pump consumes power in order to achieve the desired temperature lift. The capacity of the lunar base power station needs to be increased in order to account for this additional power consumption. It is reasonable to assume that the additional mass penalty would be proportional to the power supplied to the heat pump. A review of the literature shows that there is no consensus on the mass penalty [1-3, 6, 7, 17]. The values quoted lately are in the neighborhood of 30 kg/kW for photovoltaic or nuclear units. This value will be used in our studies. It is, however, possible to substitute other values for the specific mass in the spreadsheet and perform the analysis without difficulty.

2.6 Results

The overall mass optimization was performed using a spreadsheet. The heat pump output temperature lift, and hence the radiator temperature, was varied, and the variations of the masses of the components and the TCS were computed using the mass models described in this report. For the coupled TCS configuration, Case A, the analyses were performed for two working fluids, R11 and R717. The overall TCS mass variation as a function of radiator temperature is shown in Figure 14(a). Similar analyses were performed for the decoupled configuration, Case B [Figure 14(b)]. For Case B, R11 and R717 were used as the working fluids for the heat pump, but R717 was used in the rejection loop due to its superior heat transport characteristics.

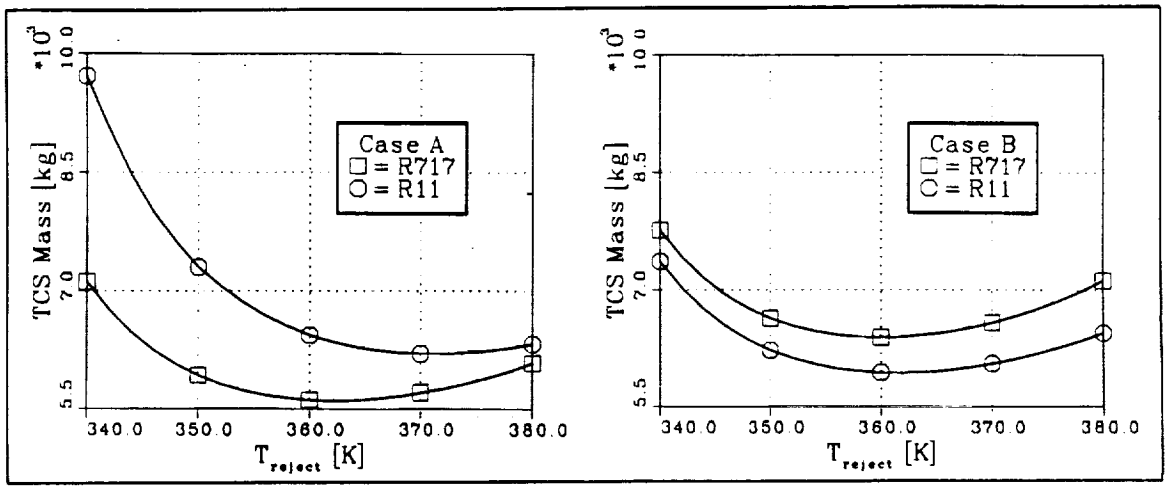

Figure 14. Overall TCS mass as a function of T_{reject}.

When R11 is used as the working fluid for the heat pump, the optimal TCS mass is 6108 kg at a radiator temperature of 371 K for the coupled situation, Case A. For Case B, the optimal TCS mass is 5940 kg at a radiator temperature of 362 K. The radiator mass in Case B is higher than in Case A because of its lower operating temperature. Also, the presence of the heat exchanger between the heat pump and the rejection loop adds extra mass to the Case B scenario. In spite of these mass penalties, the optimal TCS system mass for Case B is lower than that for Case A. This is due to the large reduction in the rejection loop piping mass for Case B. When R717 is used as the working fluid in the heat pump, the optimal mass of the TCS is 5515 kg at a radiation temperature of 362 K for Case A. For Case B, the corresponding values are 6392 kg and 360 K, respectively. It is obvious that Case B is more massive than Case A, since the radiator temperature for Case B is lower and it also has an additional heat exchanger. The masses of the individual components for Cases A and B are shown graphically in Figures 15 and 16 for a range of radiator temperatures and are listed Tables 2-7.

Among the cases considered, the R717 coupled TCS configuration offers the least mass, 5515 kg. The best decoupled configuration would involve R11 as the working fluid for the heat pump and R717 as the working fluid for the rejection loop. The

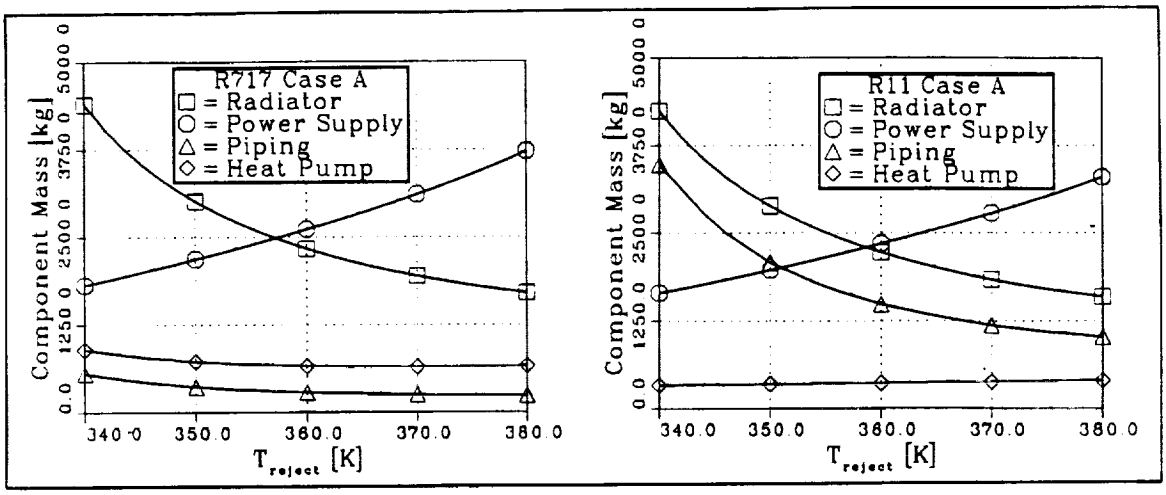

Figure 15. Component masses as a function of T_{reject} for Case A.

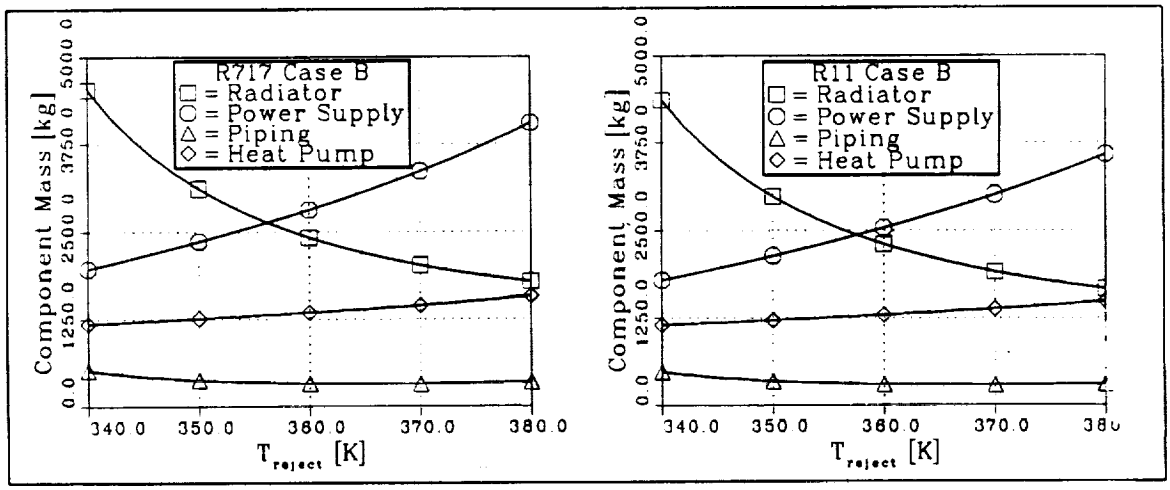

Figure 16. Component masses as a function of T_{reject} for Case B.

Table 2. Variation of TCS mass and its components with radiator temperature for R717, Case A.

Acquisition						
Cooling load	Q_{cool}	[kW]	100	100	100	100
Cooling temperature	T_{cool}	[K]	275	275	275	275
Heat Pump						
Temperature drop, HX_{in}	$\Delta T_{HX_{in}}$	[K]	5	5	5	5
Input temperature	T_{low}	[K]	270	270	270	270
Output temperature	T_{high}	[K]	**340**	**360**	**380**	**400**
Heat pump efficiency	COP	[-]	1.6467	1.1466	0.8052	0.5186
Compressor power	W_c	[kW]	60.73	87.22	124.20	192.82
Rejection heat load	Q_{reject}	[kW]	160.7	187.2	224.2	292.8
Evaporator specific mass	m_{evap}	[kg/kW]	2.72	2.72	2.72	2.72
Compressor specific mass	m_{comp}	[kg/kW]	0.202	0.202	0.202	0.202
Evaporator mass	M_{evap}	[kg]	272	272	272	272
Compressor mass	M_{comp}	[kg]	32.47	37.82	45.29	59.15
Heat pump mass	M_{HP}	[kg]	305	310	317	331
Power Supply						
Specific mass	m_{power}	[kg/kW]	30	30	30	30
Power penalty	M_{power}	[kg]	1822	2616	3726	5785
Rejection Loop						
Pipe mass	$M_{pipe\&fluid}$	[kg]	527	257	205	240
Radiator						
Rejection temperature	T_{reject}	[K]	340	360	380	400
Sink temperature	T_{sink}	[K]	320	320	320	320
Fin efficiency	η	[-]	0.7	0.7	0.7	0.7
Emissivity	ϵ	[-]	0.8	0.8	0.8	0.8
Radiator area	A	[m^2]	1759.0	934.3	681.2	610.1
Radiator specific mass	m_{rad}	[kg/m^2]	2.5	2.5	2.5	2.5
Radiator mass	M_{rad}	[kg]	4398	2336	1703	1525
System Mass		[kg]	7052	5519	5951	7881

Table 3. Optimum component and TCS masses for Case A with R717.

Acquisition Loop			
Cooling load	Q_{cool}	100	kW
Cooling temperature	T_{cool}	275	K
Heat Pump			
Temperature drop, HX_{in}	$\Delta T_{HX_{in}}$	5	K
Input temperature	T_{low}	270	K
Output temperature	T_{high}	362	K
Heat pump efficiency	COP	1.11	
Compressor power	W	90.2	kW
Rejection heat load	Q_{reject}	190.2	kW
Evaporator specific mass	m_{evap}	2.72	kg/kW
Compressor specific mass	m_{comp}	0.202	kg/kW
Evaporator mass	M_{evap}	272	kg
Compressor mass	M_{comp}	18.2	kg
Heat pump mass	M_{HP}	290	kg
Power Supply			
Specific mass	m_{power}	30	kg/kW
Power penalty	M_{power}	2707	kg
Rejection Loop			
Pipe mass	M_{pipe}	278	kg
Radiator			
Rejection temperature	T_{reject}	362	K
Sink temperature	T_{sink}	320	K
Fin efficiency	η	0.7	
Emissivity	ϵ	0.8	
Radiator area	A	895.9	m^2
Radiator specific mass	m_{rad}	2.5	kg/m^2
Radiator mass	M_{rad}	2240	kg
System Mass	M_{TCS}	5515	kg

Table 4. Variation of TCS mass and its components with radiator temperature for R11, Case A.

Acquisition						
Cooling load	Q_{cool}	[kW]	100	100	100	100
Cooling temperature	T_{cool}	[K]	275	275	275	275
Heat Pump						
Temperature drop, HX_{in}	$\Delta T_{HX_{in}}$	[K]	5	5	5	5
Input temperature	T_{low}	[K]	270	270	270	270
Output temperature	T_{high}	[K]	**340**	**360**	**380**	**400**
Heat pump efficiency	COP	[-]	1.8789	1.3266	0.9458	0.6623
Compressor power	W_c	[kW]	53.20	76.61	105.73	150.99
Rejection heat load	Q_{reject}	[kW]	153.2	175.6	205.7	251.0
Evaporator specific mass	m_{evap}	[kg/kW]	2.72	2.72	2.72	2.72
Compressor specific mass	m_{comp}	[kg/kW]	0.202	0.202	0.202	0.202
Evaporator mass	M_{evap}	[kg]	272	272	272	272
Compressor mass	M_{comp}	[kg]	30.95	35.47	41.56	50.70
Heat pump mass	M_{HP}	[kg]	303	307	314	323
Power Supply						
Specific mass	m_{power}	[kg/kW]	30	30	30	30
Power penalty	M_{power}	[kg]	1596	2268	3172	4530
Rejection Loop						
Pipe mass	$M_{pipe\&fluid}$	[kg]	3100	1243	815	712
Radiator						
Rejection temperature	T_{reject}	[K]	340	360	380	400
Sink temperature	T_{sink}	[K]	320	320	320	320
Fin efficiency	η	[-]	0.7	0.7	0.7	0.7
Emissivity	ϵ	[-]	0.8	0.8	0.8	0.8
Radiator area	A	[m^2]	1676.6	876.4	625.0	523.0
Radiator specific mass	m_{rad}	[kg/m^2]	2.5	2.5	2.5	2.5
Radiator mass	M_{rad}	[kg]	4191	2191	1563	1307
System Mass		[kg]	9190	6009	5864	6872

Table 5. Optimum component and TCS masses for Case A with R11.

Acquisition Loop			
Cooling load	Q_{cool}	100	kW
Cooling temperature	T_{cool}	275	K
Heat Pump			
Temperature drop, HX_{in}	$\Delta T_{HX_{in}}$	5	K
Input temperature	T_{low}	270	K
Output temperature	T_{high}	371	K
Heat pump efficiency	COP	1.06	
Compressor power	W	94.5	kW
Rejection heat load	Q_{reject}	194.5	kW
Evaporator specific mass	m_{evap}	2.72	kg/kW
Compressor specific mass	m_{comp}	0.202	kg/kW
Evaporator mass	M_{evap}	272	kg
Compressor mass	M_{comp}	19.1	kg
Heat pump mass	M_{HP}	291	kg
Power Supply			
Specific mass	m_{power}	30	kg/kW
Power penalty	M_{power}	2836	kg
Rejection Loop			
Pipe mass	M_{pipe}	1171	kg
Radiator			
Rejection temperature	T_{reject}	371	K
Sink temperature	T_{sink}	320	K
Fin efficiency	η	0.7	
Emissivity	ϵ	0.8	
Radiator area	A	724.2	m^2
Radiator specific mass	m_{rad}	2.5	kg/m^2
Radiator mass	M_{rad}	1810	kg
System Mass	M_{TCS}	6108	kg

Table 6. Optimum component and TCS masses for Case B with R717.

Acquisition Loop			
Cooling load	Q_{cool}	100	kW
Cooling temperature	T_{cool}	275	K
Heat Pump			
Temperature drop, HX_{in}	$\Delta T_{HX_{in}}$	5	K
Temperature drop, HX_{out}	$\Delta T_{HX_{out}}$	5	K
Input temperature	T_{low}	270	K
Output temperature	T_{high}	365	K
Heat pump efficiency	COP	1.06	
Compressor power	W	94.0	kW
Rejection heat load	Q_{reject}	194.0	kW
Evaporator specific mass	m_{evap}	2.72	kg/kW
Condenser/HX specific mass	m_{cond}	2.72	kg/kW
Compressor specific mass	m_{comp}	0.202	kg/kW
Evaporator mass	M_{evap}	272	kg
Condenser/HX mass	M_{cond}	527.8	kg
Compressor mass	M_{comp}	19.0	kg
Heat pump mass	M_{HP}	819	kg
Power Supply			
Specific mass	m_{power}	30	kg/kW
Power penalty	M_{power}	2821	kg
Rejection Loop			
Liquid pipe mass	M_{liquid}	213.3	kg
Vapor pipe mass	M_{vapor}	117.5	kg
Pipe mass	M_{pipe}	331	kg
Radiator			
Rejection temperature	T_{reject}	360	K
Sink temperature	T_{sink}	320	K
Fin efficiency	η	0.7	
Emissivity	ϵ	0.8	
Radiator area	A	968.5	m^2
Radiator specific mass	m_{rad}	2.5	kg/m^2
Radiator mass	M_{rad}	2421	kg
System Mass	M_{TCS}	6392	kg

Table 7. Optimum component and TCS masses for Case B with R11.

Acquisition Loop			
Cooling load	Q_{cool}	100	kW
Cooling temperature	T_{cool}	275	K
Heat Pump			
Temperature drop, HX_{in}	$\Delta T_{HX_{in}}$	5	K
Temperature drop, HX_{out}	$\Delta T_{HX_{out}}$	5	K
Input temperature	T_{low}	270	K
Output temperature	T_{high}	367	K
Heat pump efficiency	COP	1.14	
Compressor power	W	87.7	kW
Rejection heat load	Q_{reject}	187.7	kW
Evaporator specific mass	m_{evap}	2.72	kg/kW
Condenser/HX specific mass	m_{cond}	2.72	kg/kW
Compressor specific mass	m_{comp}	0.202	kg/kW
Evaporator mass	M_{evap}	272	kg
Condenser/HX mass	M_{cond}	510.6	kg
Compressor mass	M_{comp}	17.7	kg
Heat pump mass	M_{HP}	800	kg
Power Supply			
Specific mass	m_{power}	30	kg/kW
Power penalty	M_{power}	2631	kg
Rejection Loop			
Liquid pipe mass	M_{liquid}	193.5	kg
Vapor pipe mass	M_{vapor}	104.8	kg
Pipe mass	M_{pipe}	298	kg
Radiator			
Rejection temperature	T_{reject}	362	K
Sink temperature	T_{sink}	320	K
Fin efficiency	η	0.7	
Emissivity	ϵ	0.8	
Radiator area	A	884.2	m^2
Radiator specific mass	m_{rad}	2.5	kg/m^2
Radiator mass	M_{rad}	2211	kg
System Mass	M_{TCS}	5940	kg

optimal mass for this configuration, as stated earlier, is 5940 kg. In spite of the additional mass, the decoupled system is the preferred configuration, for the reasons cited in Section 2.3.2.

CHAPTER 3. A THERMAL CONTROL SYSTEM BASED ON AN ABSORPTION HEAT PUMP

The Rankine-cycle heat pump discussed in the previous section is an example of a work-driven heat pump (WDHP). The energy needed to accomplish the temperature lift is provided as shaft work, usually by an electrical motor driving a compressor. There is a class of heat pumps that uses high-temperature heat instead of shaft work to remove heat from a low-temperature source. These heat-driven heat pumps (HDHP) can be attractive in a scenario where a high-temperature heat source is available (such as process waste heat). Using this waste heat, the power penalty associated with the shaft work can be reduced. In the case of a lunar base, high-temperature heat may be available as a byproduct of a main electrical power unit, such as a nuclear reactor or a solar dynamic power plant. A SP-100 type nuclear reactor operating a Brayton cycle would provide, in addition to the electric power, waste heat in the megawatt range at temperatures of 600 to 1000 K [18-20]. Even in a scenario where no such heat is available, high-quality heat can be generated using solar collectors. The heat generation of a solar collector varies with the intensity of solar radiation in the same manner as the effective sink temperature of the lunar environment. Therefore, a HDHP using solar collectors is self-adaptive in the sense that most energy is provided at peak load.

The schematic for a HDHP is given in Figure 17(a). Heat supplied from the source (Q_{source} at T_{source}) is used to lift a cooling load (Q_{cool} at T_{cool}) up to a higher temperature (T_{reject}), where all heat ($Q_{source} + Q_{cool}$) is rejected. Analogous to the WDHP, the coefficient of performance of a HDHP is given by

$$COP = \frac{Q_{cool}}{Q_{source}} .$$

Figure 17(b) shows how this heat pump can be divided into a heat engine, working between T_{source} and $T_{reject1}$ and driving a heat pump between T_{cool} and $T_{reject2}$. This

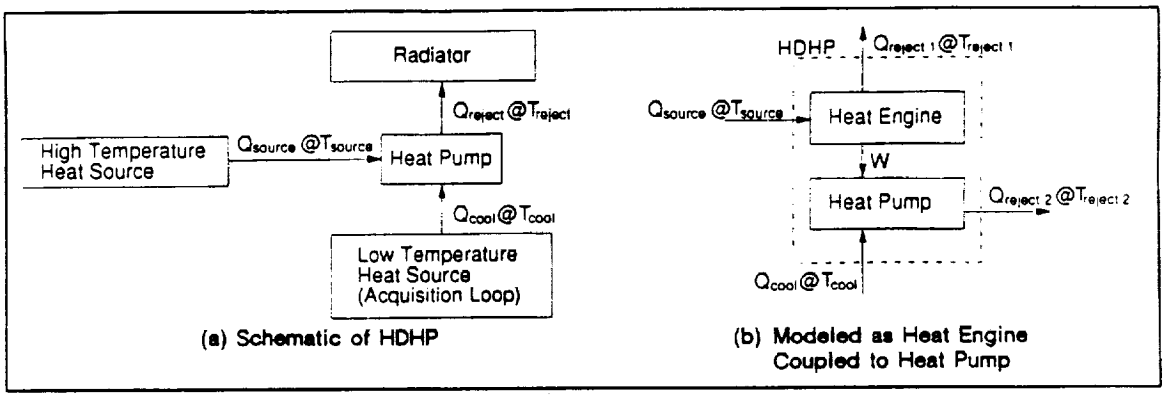

Figure 17. A heat-driven heat pump (HDHP).

model can be utilized to derive the maximum efficiency of a HDHP. Ideally, both the engine and the heat pump are Carnot cycles with

$$\eta_{engine} = \frac{T_{source} - T_{reject1}}{T_{source}}$$

$$COP_{HP} = \frac{T_{cool}}{T_{reject2} - T_{cool}}$$

and therefore

$$COP_{HDHP} = \eta_{engine} \cdot COP_{HP} = \frac{T_{source} - T_{reject1}}{T_{source}} \frac{T_{cool}}{T_{reject2} - T_{cool}} .$$

This model indicates that heat could be rejected at two different temperatures. If the heat pump is designed for a given rejection temperature, $T_{reject2}$, and T_{source} and T_{cool} are fixed, there remains the choice of the source rejection temperature, $T_{reject1}$. Choosing $T_{reject1}$ lower than $T_{reject2}$ would defeat the purpose of the heat pump, which is to elevate the temperature of rejected low-quality heat. The formula given for COP_{HDHP} indicates that when the restriction $T_{reject1} \geq T_{reject2}$ is applied, $T_{reject1} = T_{reject2}$ yields the maximum performance. Therefore, the complete system operates with a common rejection temperature, as shown in Figure 17(a). For non-ideal engines and heat pumps, $T_{reject1} = T_{reject2}$ still provides the best overall performance, given the above restrictions. For this reason, one common rejection temperature will be assumed in the following discussion.

One example of a HDHP is the absorption heat pump (Figure 18). Heat rejection and acquisition work similar to the Rankine cycle described in the previous chapter. Between states 1 and 2, the refrigerant condenses and rejects heat. From state 2 to state 3, it is throttled to lower pressure and then evaporated (3-4). The important difference from the Rankine cycle is the absence of a power-consuming compressor. Instead, the refrigerant goes into solution with a carrier fluid in the absorber (4-5), is pumped up to the high-pressure level (5-6), and is then separated from the carrier fluid at the higher pressure by means of heat addition (6-1) in the generator. A relatively weak solution is circulated back from the generator to the absorber (7-8). The power needed to pump the liquid is negligible compared to the compressor work of the Rankine cycle. The amount of heat spent to separate the solution in the generator is considerable. Heat will be rejected from the condenser and from the absorber. Two fluids circulate in the heat pump. One is the actual refrigerant; the other is a liquid used to absorb the refrigerant. Common pairs of working fluids are lithium bromide-water and ammonia-water. There are many other possible pairs of working fluids, but they are still in the research stages. In the following, both ammonia-water and lithium bromide-water systems will be discussed.

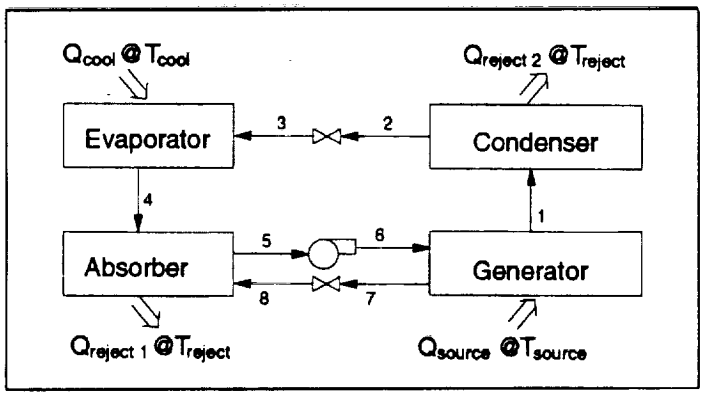

Figure 18. Schematic of an absorption heat pump.

3.1 Ammonia-Water Heat Pump

Even the simplest setup of an ammonia-water heat pump is more complex than the basic absorption pump presented in Figure 18. The additional complexity is due to the separation of ammonia and water. If an ammonia-water solution is heated to the two-phase region, the resulting vapor mixture generally contains water in addition to ammonia. Even small fractions of water in the vapor can have a considerable effect on the condenser and evaporator temperatures. As little as 0.5 mass percent water can cause a 10 K drop in the condenser temperature. Dephlegmators are used to rid the vapor mixture of water. The incoming vapor mixture is cooled with a cooling coil. The condensate contains more water than the original vapor mixture, and the remaining vapor contains a higher percentage of ammonia.

Figure 19 depicts a simple ammonia-water heat pump (thermodynamic states are denoted by numbers and the heat loads by capital letters). It will become apparent in the following discussion why a three-stage dephlegmator is used.

An enthalpy-concentration diagram of the thermodynamic processes is given in Figure 20. The dashed lines denote the two-phase region at the low-pressure level, and the dash-dotted lines denote the high-pressure saturation lines. Constant-temperature levels at the high-pressure level are denoted by dotted lines. The solid lines mark a thermodynamic process corresponding to the setup shown in Figure 19. The two-component, two-phase mixture has both components (water and ammonia) in both the liquid and the vapor phases. The state point of the mixture is represented on the diagram by n. The states of the vapor and the liquid phases are denoted by subscripts g and l, respectively. For example, for state 7, the concentration of the liquid mixture is obtained by the intersection of the isotherms with the saturated liquid line ($7l$), and the concentration of the gaseous mixture is given by $7g$ (the intersection of the isotherm with the saturated vapor line). Physically, the isotherms do not end at the saturation line; they are truncated here for clarity.

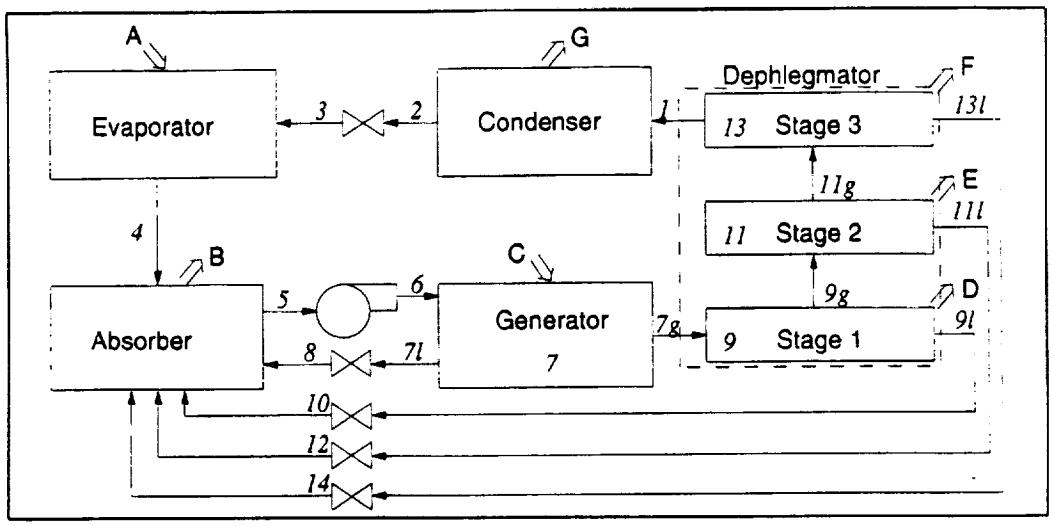

Figure 19. Schematic of a simple ammonia-water absorption heat pump.

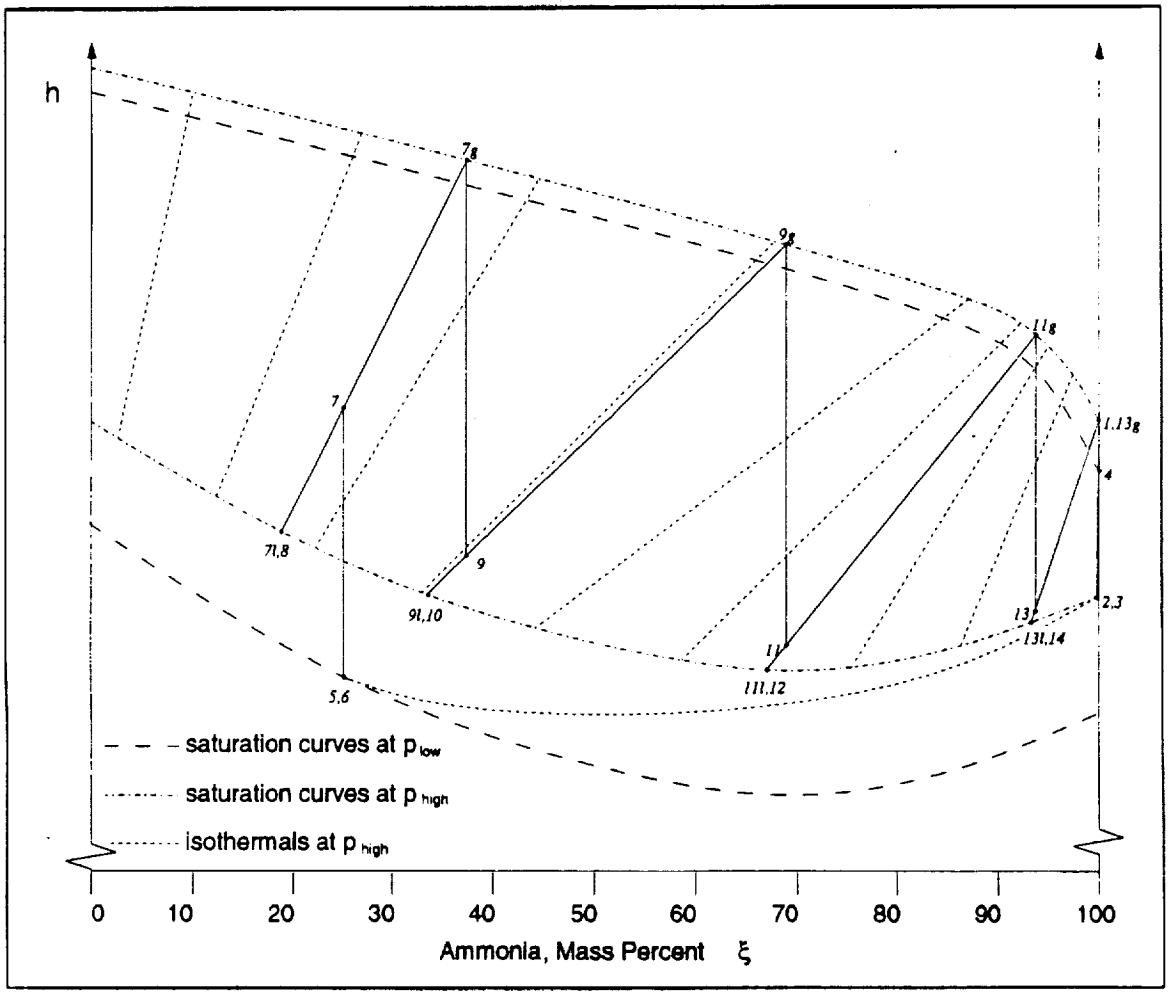

Figure 20. An enthalpy-concentration diagram of an ammonia-water absorption cycle (state numbers correspond to Figure 19).

The fluid circulating through the condenser and the evaporator can be approximated as pure ammonia. In reality, it is impossible to achieve total separation, but with proper design, the vapor quality can be high enough (≅ 99.9 mass percent) to justify this approximation. System requirements dictate the cooling and rejection temperatures, which in turn define their respective saturated pressure levels, p_{low} and p_{high}. Thus, states 1 to 4 are defined.

At state 5, the strong solution leaving the absorber has to be all liquid in order to avoid cavitation in the pump. This implies that state 5 has to be at or below the saturated liquid line for p_{low} in the h-ξ diagram (Figure 20). State 5 also defines the rejection temperature of the absorber. The mixture in the absorber has to be cooled down to state 5. This temperature would optimally be equal to the condenser temperature. Therefore, state 5 is located at the intersection of the isothermal line at condenser temperature and the saturated or subcooled liquid curve at p_{low}. In Figure 20, state 5 is at the saturated liquid curve. [The liquid in state 5 at the subcooled state is shown in Figure 21(a)]. If ξ_5 were chosen to be lower than shown in Figure 20, the absorber rejection temperature would be higher, but the separation of ammonia and water would require more energy and equipment. If ξ_5 were higher, the absorber's rejection temperature would be lower than the condenser's, thus reducing the overall system performance. The enthalpy change over the pump is negligible. Therefore, state 5 is almost identical to state 6 in the h-ξ diagram (Figure 20). The strong solution is in a subcooled state at p_{high}.

State 7 has to be at the same concentration as states 5 and 6 and within the high-pressure two-phase region. The position of state 7 in the two-phase region is proportional to the heat added to the mixture in the generator. The choice of the amount of heat to be added to the mixture is illustrated in Figure 21(b). If heat were added until the mixture is at state 7', then the concentration of the vapor mixture would be 7'*g*. The purity of the ammonia would be very low for a practical system. If the

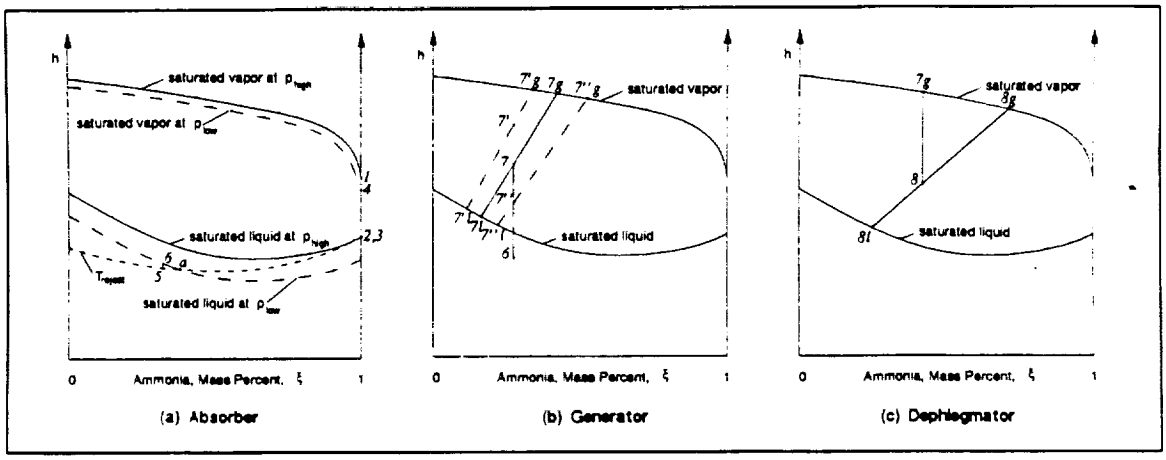

Figure 21. Enthalpy-concentration diagrams of ammonia-water absorption cycle processes.

heat added in the generator caused the mixture to be at state 7", then vapor with higher ammonia concentration (7"g) would be produced, but the mass rate of vapor production would be small due to the small amount of heat added. The operating value of state 7 has to be in between 7' and 7". To determine the optimal amount of heat to be added in the generator, and therefore the optimal state 7, would require an elaborate multiple-parameter nonlinear optimization, which is beyond the scope of this investigation.

The liquid left in the generator is throttled to p_{low} (state 8) and returned to the absorber. In the first dephlegmator stage, the vapor is cooled from state 7g to 9 using cooling coils. The selection of state 9 follows an argument presented for state 7 (generator), as can be seen in Figure 21(c).

A thermodynamic analysis indicated that three dephlegmator stages are necessary in order to obtain a 99.9 percent ammonia concentration in the vapor mixture. The dephlegmator stages 2 and 3 work analogous to stage 1. The liquids at states 8, 10, 12, and 14 and the vapor at state 4 are fed back into the absorber. Tables 8 and 9 show a practical example for this cycle. The property values were obtained from the ASHRAE handbook [21]. The data are for 1 lb/s of ammonia flow in the evaporator

Table 8. Thermodynamic states in an ammonia-water absorption cycle.

State[a]	Description	T (F)	h (Btu/lb)	p (psi)	ξ (%)	m (lb/s)
1	Condenser input	160	555	500	99.9	1.000
2	Condenser output	160	155	500	99.9	1.000
3	Evaporator input	20	155	50	99.9	1.000
4	Absorber input	20	540	50	99.9	1.000
5	Strong solution out	160	55	50	25.0	29.594
6	Strong solution in	160	55	500	25.0	29.594
7	Two phase in generator	380	440	500	25.0	29.594
7*l*	Weak solution out	380	325	500	17.0	23.819
8	Weak solution in	380	325	50	17.0	23.819
7*g*	Input dephlegmator stage 1	380	880	500	58.0	5.774
9	Two phase in dephlegmator stage 1	260	255	500	58.0	5.774
9*l*	Output solution dephlegmator stage 1	260	145	500	47.0	4.504
10	Throttled solution dephlegmator stage 1	260	145	50	47.0	4.504
9*g*	Out dephlegmator stage 1, in stage 2	260	630	500	97.0	1.270
11	Two phase in dephlegmator stage 2	180	495	500	97.0	1.270
11*l*	Output solution dephlegmator stage 2	180	120	500	82.0	0.181
12	Throttled solution dephlegmator stage 2	180	120	50	82.0	0.181
11*g*	Out dephlegmator stage 2, in stage 3	180	570	500	99.5	1.089
13	Two phase in dephlegmator stage 3	163	295	50	99.5	1.089
13*l*	Output solution dephlegmator stage 3	163	140	500	95.0	0.089
14	Throttled solution dephlegmator stage 3	163	140	50	95.0	0.089

[a] The state point numbers correspond to those given in Figure 20.

Table 9. Heat loads of the components of an ammonia-water absorption cycle.

	Description	Q (Btu/lb)	T_{low} (F)	T_{high} (F)
A	Cooling load	385	20	20
B	Absorber rejection load	7341	160	380
C	Generator load	11195	160	380
D	Dephlegmator stage 1 rejection	3628	260	380
E	Dephlegmator stage 2 rejection	158	180	260
F	Dephlegmator stage 3 rejection	53	163	180
G	Condenser rejection	400	160	160

and condenser (they are in British units, as in the handbook). The overall efficiency is

$$COP = \frac{q_{cool}}{q_{generator}} = 0.0344 .$$

Even with an optimization of the positions of states 7, 9, 11, and 13, major improvements do not seem feasible.

There is, however, a potential for slight improvement by reusing heat within the heat pump, i.e., using recovery heat exchangers to reuse the heat. Waste heat can be recovered gainfully when it is available at a high temperature. However, when a small amount of heat is involved, such as from the stage 3 dephlegmator, the associated mass penalty of the recovery heat exchangers makes its reuse worthless. Therefore, a new, improved heat pump (Figure 22) was considered. In order to reduce the rejection load of the absorber, the fluid leaving the pump is preheated by the fluid leaving the generator. Thus, the fluid entering the absorber from the generator is noticeably cooler. A second preheater uses the rejection load from the first dephlegmator stage. The modified system was evaluated based on the results shown in Table 8. For an ideal heat exchanger ($T_{6a} = T_{7/b}$), 5835 Btu/s can be transferred in the first preheater

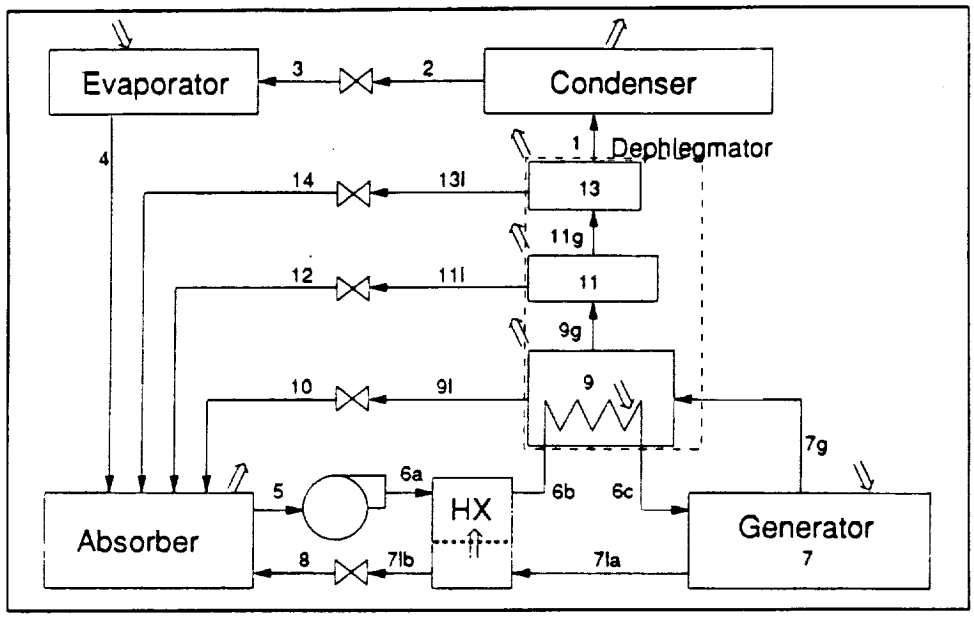

Figure 22. Schematic of an ammonia-water absorption heat pump with internal heat reuse.

and 1501 Btu/s in the second (here, $T_{6b} = T_{9l}$). The COP of this improved heat pump increases to 0.0998. Due to the very low COP of the ammonia-water absorption heat pump, a mass analysis has not been performed for the system.

3.2 Lithium Bromide-Water Heat Pump

A common absorption system for terrestrial applications uses a lithium bromide and water mixture. Similar to the ammonia-water system, the compressor work of the Rankine cycle is replaced by heat-operated pressurization processes. The lithium bromide-water system is popular because of the relative ease with which the refrigerating fluid (water) can be separated in pure form from the carrier fluid (lithium bromide). The basic principle of operation of the cycle is similar to that of the ammonia-water system described earlier. A brief description of the components and processes follows.

Figure 23 depicts a schematic of a lithium bromide-water absorption heat pump. Here, superheated steam at high pressure (state 1) leaves the generator and condenses

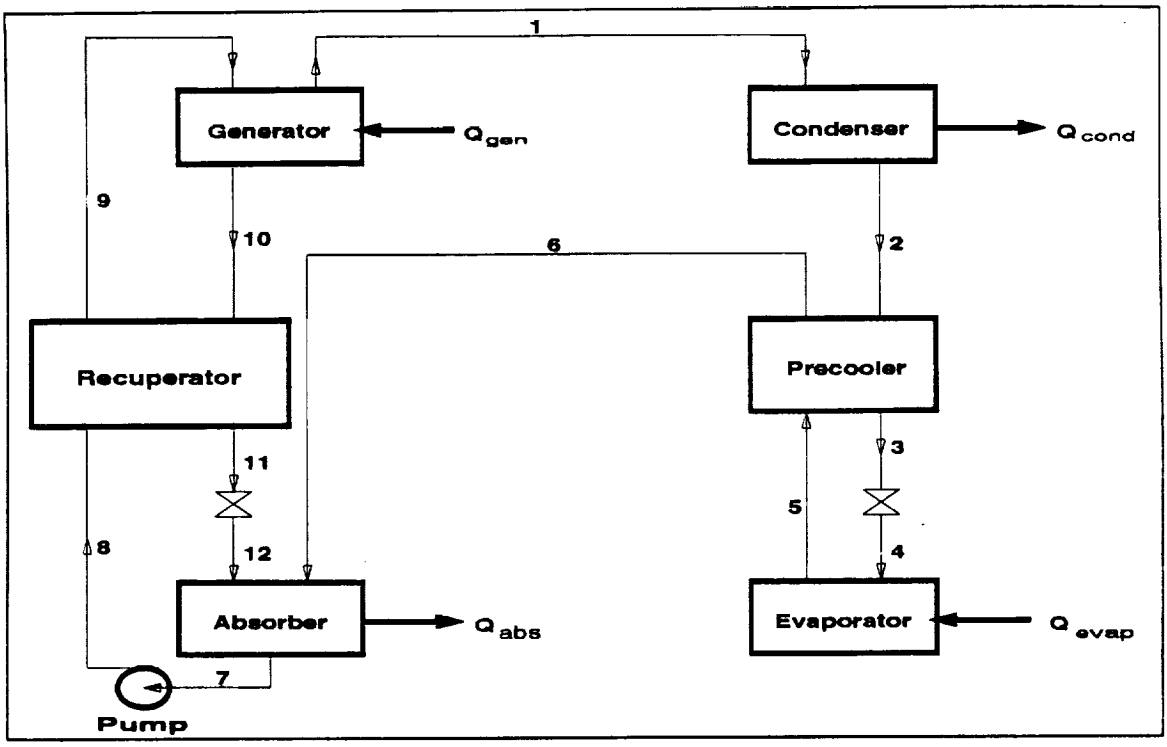

Figure 23. Schematic of a simple lithium bromide-water absorption heat pump.

to saturated liquid in the condenser (state 2). The liquid is subcooled in the precooler (state 3) and expands in the valve to form a low-pressure liquid-vapor mixture (state 4). This mixture absorbs the heat to be removed and forms saturated vapor at low pressure in the evaporator (state 5). The vapor absorbs heat in the precooler to form supersaturated vapor (state 6) and then enters the absorber.

In the absorber, the supersaturated steam mixes with the high-concentration (strong) lithium bromide-water solution (state 12). The concentration of the solution is changed to state 7. The heat of condensation and heat of solution are removed from the absorber using cooling coils. The low-pressure solution is pumped to higher pressure, and the subcooled solution absorbs heat in a recovery heat exchanger. The weak solution enters the generator, where heat is added in order to separate pure steam from the solution. The strong solution (state 10) rejects heat in the heat exchanger, expands to low pressure in a valve, and re-enters the absorber, thus completing the cycle.

In the cycle just described, the cooling-load heat is absorbed by the evaporator, and is raised to a higher temperature and rejected by the condenser. In order to achieve this end, high-temperature heat is supplied to the generator. In addition, the cycle mandates that the heats of condensation and solution be rejected from the absorber. A detailed cycle analysis follows.

The system depicted in Figure 23 can be completely defined thermodynamically if the following parameters are specified: (1) Q_{cool}, the cooling load; (2) T_{cool}, the acquisition temperature of the cooling load; (3) T_{gen}, the generator operating temperature; (4) ξ_{strong}, the concentration of the strong solution; and (5) ξ_{weak}, the concentration of the weak solution. In other words, for a given capacity (Q_{cool}), the designer of the system has four degrees of freedom. In the case of a TCS for the lunar base, as with most TCS applications, T_{cool} is specified based on the application--270 K for lunar base needs and 280 K due to working fluid restrictions for this system. For the LiBr-water system, the initiation of crystallization sets an upper bound on ξ_{strong}. Hence, the degrees of freedom are reduced to two, viz., ξ_{weak} and T_{gen}. It would be a straightforward process to generate the COP of the system as a function of these two parameters. However, from a TCS design perspective, it is desirable to obtain COP as a function of the rejection temperature, T_{high}. The following procedure is adapted in order to attain this relationship.

Figure 24 shows the variation of COP with ξ_{weak}, the weak solution concentration, for generator temperatures of 500, 600, and 700 K. It can be seen that the weaker the concentration, the better the COP of the system. Hence, for better performance, it is desirable to operate the cycle with the weak solution concentration as low as permissible. The variation of T_{high} with ξ_{weak} for generator temperatures of 500, 600, and 700 K is shown in Figure 25. It can be seen that there is a one-to-one correspondence between ξ_{weak} and T_{high} in the region of $\xi_{weak} \leq 60\%$. As demonstrated in Figure 24, it is preferable to maintain ξ_{weak} as low as practical. Hence, in the region of interest, we express ξ_{weak} as a function of T_{high} for a given T_{cool} and T_{gen}. In other words, COP can be specified in terms of T_{high} and T_{gen}.

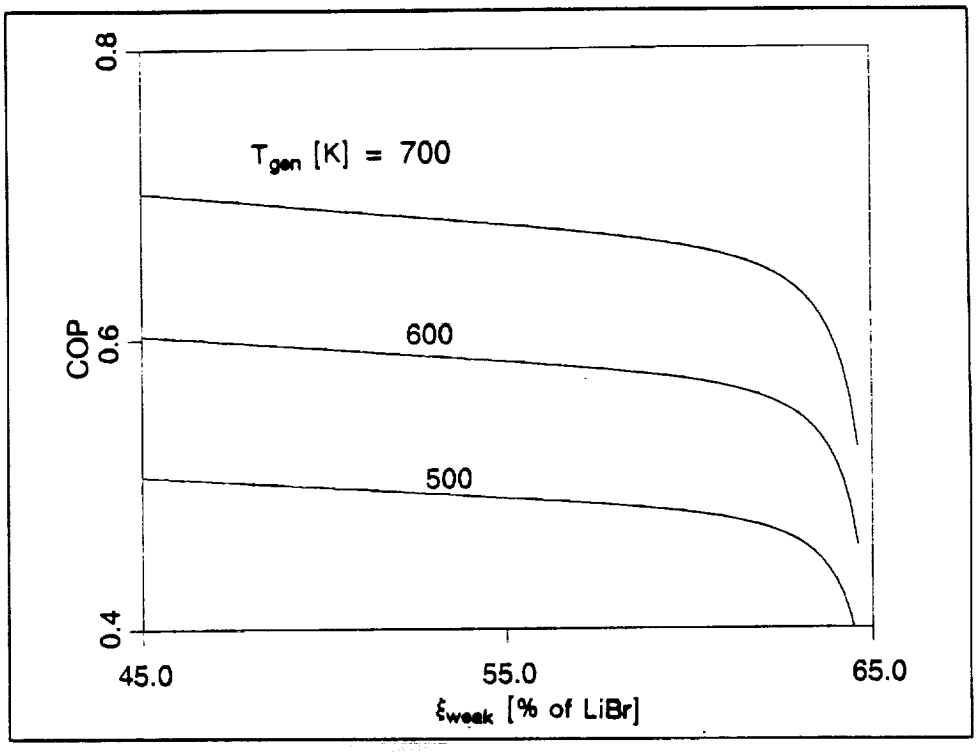

Figure 24. Variation of COP with ξ_{weak} (T_{gen} = 500, 600, and 700 K).

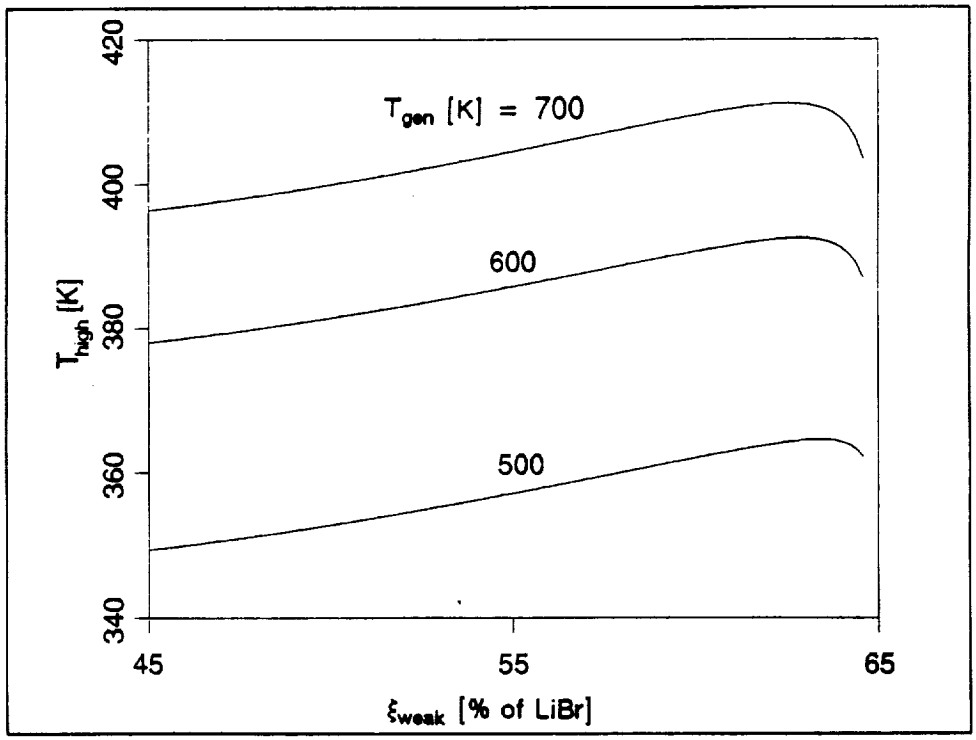

Figure 25. Variation of T_{high} with ξ_{weak} (T_{gen} = 500, 600, and 700 K).

Figure 26 is a plot of the COP as a function of T_{gen} for T_{high} = 360–400 K (T_{cool} = 280 K). It can be seen that, for any given T_{high}, there is a distinct maximum for the COP. In this analysis, we have assumed that the T_{gen} value corresponding to this maxima is a feasible value for the cycle. It is simple to verify this assumption, once the cycle analysis is completed using the value. If we pick these maximum values for T_{gen} from Figure 26, then the COP can be computed as a function of T_{high} alone. Using the technique described above, the COP values are computed for a few rejection temperatures in the range of 360 to 400 K. It is found that a linear fit can be obtained for the computed values, as shown in Figure 27. The cycle analysis and mass estimates are now performed with the radiator temperature (T_{high}) as the free variable. The COP values used for the mass analysis are obtained from Figure 27.

In the analysis, a common rejection temperature has been assumed for the absorber and condenser. The validity of this assumption has been discussed in an earlier section. It should also be noted that, since water is used as the coolant in the system, it is not possible to operate this TCS with a T_{cool} of 270 K. T_{cool} = 280 K has been assumed for this analysis. This increased acquisition temperature may be unacceptable for some sensor cooling needs in the base. Similar to Case B for the Rankine-cycle TCS, the condenser is decoupled from the rejection loop. Such a decoupling would allow the designer to operate multiple heat pumps (with potentially different values for T_{cool}) and connect them to a common rejection loop. From both control and safety perspectives, a decoupled system is better. It is also possible to use a better working fluid, ammonia, for the rejection loop with the decoupling.

The specific masses of the various absorption cycle components are not readily available. However, the major components of the heat pump (evaporator, condenser, absorber, generator, precooler, and recuperator) can all be approximated as heat exchangers and their masses estimated based on the rate of heat transfer occurring inside them. Such an approximation, though simplistic, would provide a mass estimate

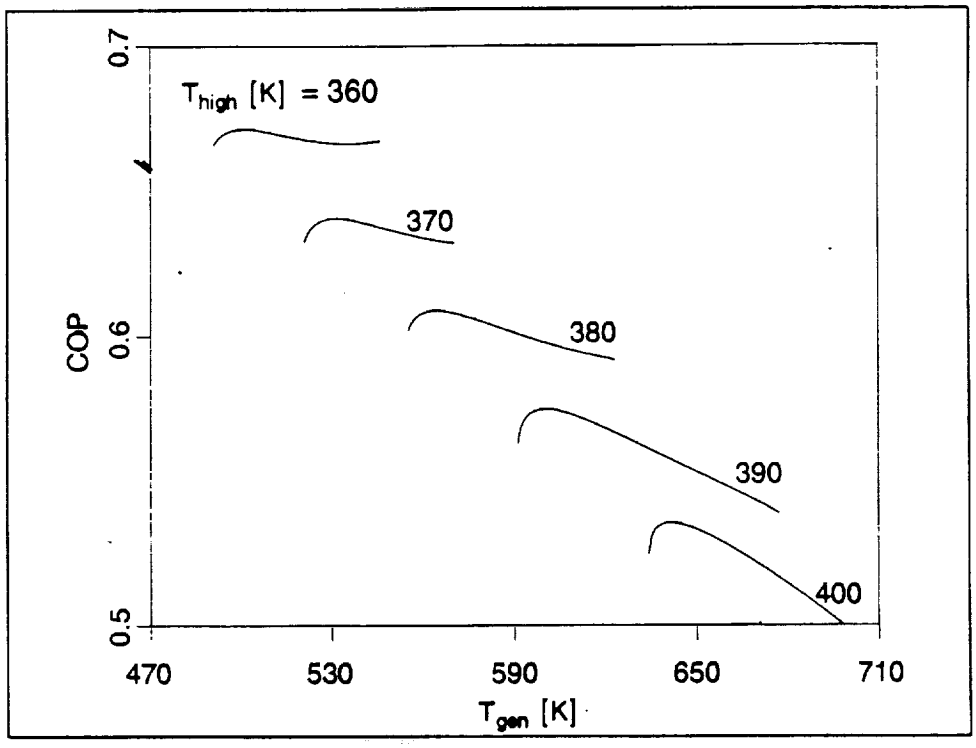

Figure 26. Variation of COP with T_{gen} (T_{high} = 360-600 K, T_{cool} = 280 K).

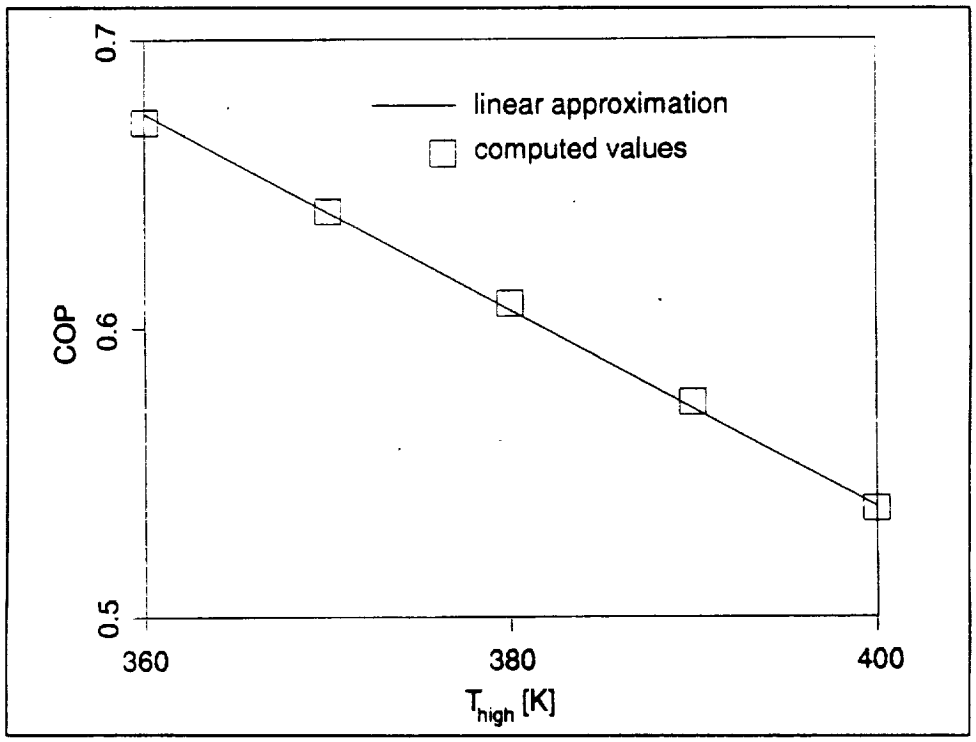

Figure 27. Variation of COP with T_{high} for the LiBr-water absorption pump.

that would benefit this cycle, since it would underpredict the mass of the components. Hence, it could be called an optimistic mass estimate.

At this juncture, the heat loads to all the components need to be estimated in order to predict the mass of the heat pump. Table 10 provides a complete cycle analysis for T_{high} = 360, 380, and 400 K. This analysis provides the heat loads to all the heat pump components. The mass of the components can be computed by multiplying the heat loads by the specific mass of the heat exchangers (2.72 kg/kW in this case). Intermediate values can be computed numerically in exactly the same manner. Rather than computing the heat loads at every rejection temperature by means of the laborious cycle analysis, a simpler scheme was devised using the following arguments. From Table 10, it can be seen that the heat input to the generator and evaporator equals the heat rejected at the condenser and absorber. This can also be seen easily from Figure 23, by performing an energy balance for the system. Hence,

$$Q_{evap} + Q_{gen} = Q_{cond} + Q_{abs} .$$

Equivalently,

$$Q_{evap} + Q_{gen} + Q_{cond} + Q_{abs} = 2(Q_{evap} + Q_{gen}) = 2Q_{cool}\left[1 + \frac{1}{COP}\right] .$$

The amount of heat recovery that occurs in the recuperator and precooler can be determined by performing a cycle analysis as shown in Table 10. The sum of the heat loads in the recuperator and precooler will be termed the internal heat load, Q_{int}. The internal heat loads at T_{high} of 360, 380, and 400 K are listed, along with Q_{gen}, in Table 11. An effort was made to see if a simple proportionality constant existed between Q_{gen} and Q_{int}, i.e., $Q_{int} = k \cdot Q_{gen}$. The values of k are also listed in Table 11. It can be seen that no simple constant can be used for the range of interest. It was found, however, that the value of k did not change appreciably for small variations in T_{high}. Hence, the approach used to calculate Q_{int} was to determine k for a narrow range of

Table 10. LiBr-water absorption heat pump cycle analysis.

a. State Point Properties.

	T [K]			p [kPa]			x			ξ [%]			ṁ [kg/s]			h [kJ/kg]		
T_{high} [K]	360	380	400	360	380	400	360	380	400	360	380	400	360	380	400	360	380	400
State 1[a]	501.0	564.0	641.0	446.09	1545.658	4940.539	1.000	1.000	1.000	0.0	0.0	0.0	0.0466	0.0496	0.0543	2916.2	3015.4	3115.9
2	420.8	472.9	536.4	446.09	1545.658	4940.538	0.000	0.000	0.000	0.0	0.0	0.0	0.0466	0.0496	0.0543	621.4	851.4	1150.8
3	360.6	391.1	431.6	446.09	1545.658	4940.539	0.000	0.000	0.000	0.0	0.0	0.0	0.0466	0.0496	0.0543	365.9	495.6	670.9
4	280.0	280.0	280.0	0.99	0.991	0.991	0.136	0.188	0.259	0.0	0.0	0.0	0.0466	0.0496	0.0543	365.9	495.6	670.9
5	280.0	280.0	280.0	0.99	0.991	0.991	1.000	1.000	1.000	0.0	0.0	0.0	0.0466	0.0496	0.0543	2513.5	2513.5	2513.5
6	415.8	467.9	531.4	0.99	0.991	0.991	1.000	1.000	1.000	0.0	0.0	0.0	0.0466	0.0496	0.0543	2769.1	2869.3	2993.4
7	314.3	316.6	319.3	0.99	0.991	0.991	0.000	0.000	0.000	57.3	58.5	59.8	0.3952	0.4948	0.6832	105.1	114.8	126.7
8	314.3	316.6	319.3	446.09	1545.658	4940.539	0.000	0.000	0.000	57.3	58.5	59.8	0.3952	0.4948	0.6832	105.1	114.8	126.7
9	457.2	514.3	589.0	446.09	1545.658	4940.539	0.000	0.000	0.000	5703	58.5	59.8	0.3952	0.4948	0.6832	392.7	506.5	650.6
10	501.0	564.0	641.0	446.09	1545.658	4940.539	0.000	0.000	0.000	65.0	65.0	65.0	0.3486	0.4452	0.6289	482.9	596.2	734.9
11	319.3	321.6	324.3	446.09	1545.658	4940.539	0.000	0.000	0.000	65.0	65.0	65.0	0.3486	0.4452	0.6289	156.9	161.0	165.8
12	319.3	321.6	324.3	0.99	0.991	0.991	0.000	0.000	0.000	65.0	65.0	65.0	0.3486	0.4452	0.6289	156.9	161.0	165.8

b. COP and Heat Loads.

			T_{high} [K]: 360	380	400
Heat pump efficiency	COP		0.671	0.913	0.535
Carnot efficiency	COP_{carnot}		0.985	0.913	0.877
% of Carnot efficiency	$COP_{rel(\%)}$		68.159	66.635	61.023
Evaporator load	Q_{evap}	[kW]	100.00	100.00	100.00
Condenser load	Q_{cond}	[kW]	106.85	107.24	106.65
Generator load	Q_{gen}	[kW]	148.95	164.29	186.80
Absorber load	Q_{abs}	[kW]	142.09	157.05	180.15
Recuperator load	Q_{rec}	[kW]	113.64	193.78	357.91
Pre-cooler load	Q_{pre}	[kW]	11.90	17.63	26.04

[a] State numbers correspond to Figure 23.

Table 11. Internal heat loads in a LiBr-water system.

T_{high} [K]	Q_{cool} [kW]	Q_{int} [a] [kW]	Q_{gen} [kW]	$K = \frac{Q_{internal}}{Q_{gen}}$
360	100	124	149	0.832
380	100	210	164	1.280
400	100	383	187	2.048

[a] $Q_{int} = Q_{rec} + Q_{pre}$.

T_{high} and use that value. The total heat loads are therefore given by

$$Q_{total} = Q_{evap} + Q_{gen} + Q_{cond} + Q_{abs} + Q_{int}$$

$$= 2Q_{cool}\left[1 + \frac{1}{COP}\right] + k \cdot Q_{gen}$$

$$= Q_{cool}\left[2 + \frac{2 + k}{COP}\right],$$

where k is determined for a narrow range of T_{high}. For example, at T_{high} = 400 K, k = 2 and $Q_{total} = Q_{cool}(2 + 4/COP)$. The simplified mass of the heat pump is determined as

$$M_{HP} = (2.72\ kg/kW) \cdot Q_{total}\ .$$

3.2.1 Transport Loop from Source to Heat Pump

The transport loop connects the high-temperature heat source (such as waste heat from a power plant) to the heat pump and differs from the rejection loop of the Rankine cycle discussed previously in the following aspects:

1. Waste heat may be available at a temperature higher than the generator operating temperature. The loop need not be close to isothermal, therefore, and superheating and subcooling of the transport fluid may be permitted, instead.

2. The transport loop will operate at much higher temperatures than typical rejection loops. Since ammonia is not suited for temperatures that will be in the range of 500 to 1000 K, water, which has a high enough critical temperature, has no toxicity, and has a large latent heat capacity, can be substituted for the ammonia.

In the mass estimate, the mass of the tubes, the fluids in the tubes, a pump, and the power penalty associated with the pump are included. The operating conditions are defined by the waste heat source temperature, the generator temperature, and the pressure in the loop. The saturation pressure of the transport fluid at generator temperature provides the largest enthalpy difference for given supply and return temperatures. This yields the lowest mass flow rate and also the lowest overall mass. It is possible to pressurize the loop even higher in order to reduce the density of the steam in the supply line and therefore the size of the tubing, but the decrease in available enthalpy difference, as well as increased tube thickness, increases overall mass. The length of the piping, which is the distance between the waste heat source and the heat pump, is assumed to be 500 m. This distance is chosen for safety considerations, as the source will most likely be a nuclear reactor. The tube diameter is optimized with respect to overall mass. If the tubes are too small, the pump mass will become too large. If they are too large, the pipes will be too heavy. In all cases, the overall pressure drop in the piping is restricted to a maximum of 10 percent. Table 12 gives an example of a piping layout. The model shows low sensitivity to the available source temperature and operating pressure, as long as the pressure is above saturation pressure at generator temperature. The mass model can be linearized for use in the overall TCS optimization:

$$\dot{M}_{s,loop} = 2.9 \text{ kg/kW} \cdot \dot{Q}_{source} .$$

Table 12. Piping data for the rejection and heat source transport loops.

Loop	rejection		heat source	
Refrigerant	R717		R718	
Heat load (kW)	490		390	
Length, one way (m)	556		500	
Pressure (MPa)	6.61		9.5	
$h_g - h_f$ (kJ/kg)	697.5		2370.4	
Mass flow rate (kg/s)	0.70		0.165	
State of fluid	liquid	gas	liquid	gas
Temperature (K)	376	376	570	900
Vicosity (kg/ms)	0.645e-4	0.131e-4	0.910e-4	0.336e-4
Density (kg/m^3)	448.8	59.4	721.7	23.82
Volume flow rate (m^3/s)	1.565e-3	1.183e-2	2.280e-4	6.908e-3
Reynolds number	345000	1011000	119000	130000
Inner diameter (mm)	40	68	19.4	48.0
Velocity (m/s)	1.23	3.28	0.78	3.83
Friction factor	0.0141	0.0116	0.0174	0.0170
Pressure drop (MPa)	0.665	0.304	0.94	0.31
Wall thickness (mm)	1.66	2.80	1.15	2.84
Mass tubes (kg)	326	928	97.8	599.5
Mass fluid (kg)	317	119	106.1	21.5
Pump mass (kg)	29		19	
Power penalty (kg)	432		258	
Overall mall (kg)	2282		1130	
Specific mass (kg/kW)	4.66		2.90	

The proportionality constant is obtained using reference conditions close to optimum for the overall TCS mass (Q_{source} = 190 kW, T_{source} = 700 K, T_{gen} = 641 K, P = 9.5 MPa).

3.2.2 Rejection Loop

The mass model for the rejection loop has been discussed in detail for the Rankine-cycle heat pump decoupled from the radiators. It has been linearized for use in the overall TCS mass optimization. In order to minimize the error committed with this linearization, the conditions for the reference computation are iteratively adjusted to the minimum overall TCS mass conditions. This guarantees that the most important result of the optimization, which is the minimum overall mass, is consistent with results for the Rankine-cycle TCS. The mass of the rejection loop is

$$M_{r.loop} = 4.66 \text{ kg/kW} \cdot Q_{reject} .$$

A sensitivity analysis showed that the variation in specific mass is minimal with modest variation in optimal working conditions. Table 12 presents data for the piping at the mass optimal reference condition.

3.2.3 Radiators

The mass model for the radiator was discussed in detail in a previous section. The parameters for the model are the same as for the Rankine TCS and are summarized in Table 13. The mass of the radiator rejecting Q_{source} at T_{source} would be a part of the power supply radiator under normal circumstances. When a TCS utilizes this heat, as in the case of the HDHP, the mass of the power supply radiator is reduced by a quantity proportional to Q_{source}. This is accounted for in the TCS optimization for the HDHP.

Table 13. Radiator parameters.

Sink temperature	T_{sink} = 320 K
Emissivity	ϵ = 0.8
Fin efficiency	η = 0.7
Specific radiator mass	m_{rad} = 2.5 kg/m^2

The variation of TCS mass with the radiator temperature is plotted in Figure 28. It is noted that the minimum TCS mass of about 6000 kg is at 396 K. The component masses for this optimal case are listed in Table 14. It must be recalled that the following assumptions were made in the mass calculations: (1) The actual hardware for the heat pump was approximated as heat exchangers, thus underestimating the mass of the components. (2) In addition, it has been assumed that no pressure drops occur in the components of the heat pump. This, again, causes an underestimation of the mass of the heat pump. (3) The use of water as the refrigerant restricted T_{cool} to 280 K, and the mass analysis was performed using this value rather than T_{cool} = 270 K as for the Rankine cycle. (4) No mass penalty has been assigned for the heat source. For these reasons, it is concluded that the Rankine cycle described in Chapter 2 would be a more optimal cycle than the absorption cycles described here.

Table 14. Optimum component and TCS masses for a LiBr-water absorption heat pump.

Acquisition Loop			
Cooling load	Q_{cool}	100	kW
Cooling temperature	T_{cool}	280	K
Heat Pump			
Output temperature	T_{high}	401	K
Heat pump efficiency	COP	0.535	
Heat source	Q_{gen}	186.87	kW
Rejection load	Q_{reject}	286.87	kW
Heat pump mass	M_{HP}	2577	kg
Heat Source			
Source temperature	T_{source}	700	K
Source load	Q_{gen}	186.87	kW
Source loop specific mass	$m_{s.loop}$	2.9	kg/kW
Source loop mass	$M_{s.loop}$	542	kg
Rejection Loop			
Rejection load	Q_{reject}	286.87	kW
Rejection loop specific mass	$m_{r.loop}$	4.66	kg/kW
Rejection loop mass	$M_{r.loop}$	1337	kg/kW
Radiator			
Rejection temperature	T_{reject}	401	K
Sink temperature	T_{sink}	320	K
Fin efficiency	η	0.7	
Emissivity	ϵ	0.8	
Radiator area	A	640.5	m^2
Radiator specific mass	m_{rad}	2.5	kg/m^2
Radiator mass	M'_{rad}	1601.25	kg
Power radiator mass savings	M_{rad-}	64.13	kg
Net radiator mass (M'_{rad}-M_{rad-})	M_{rad}	1537	kg
System Mass	M_{TCS}	5993	kg

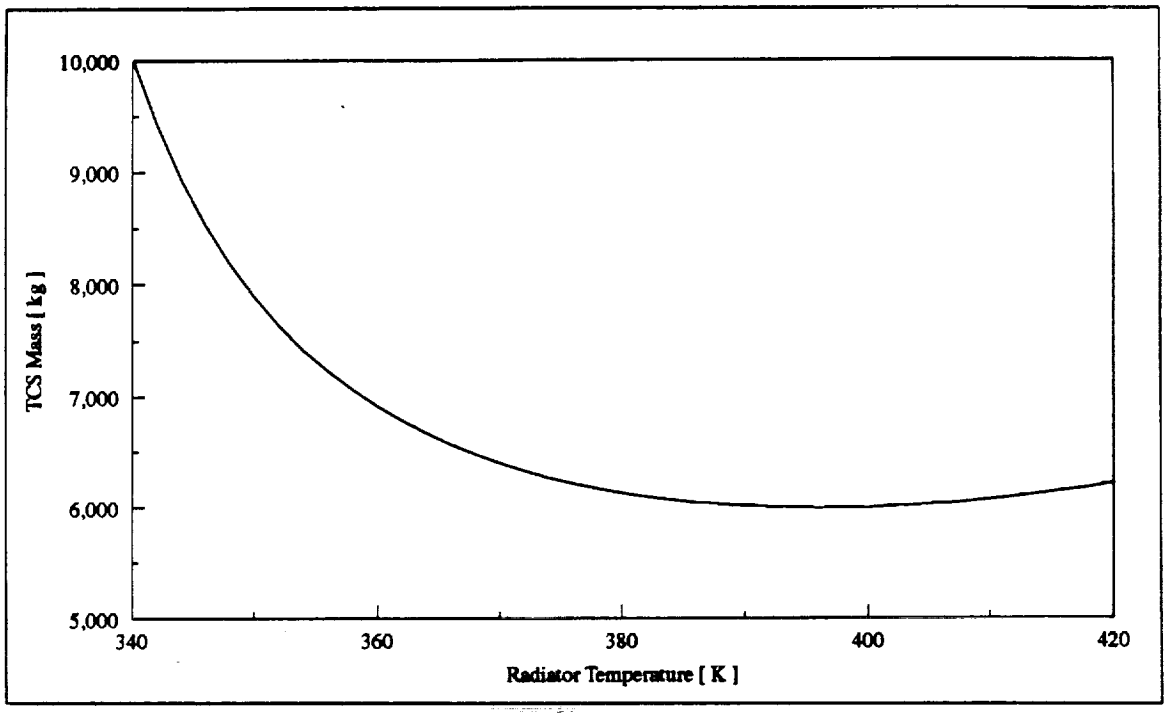

Figure 28. Variation of TCS mass with radiator temperature.

REFERENCES

1. T. D. Swanson, R. Radermacher, F. A. Costello, J. S. Moore, and D. R. Mengers, "Low-Temperature Thermal Control for a Lunar Base," SAE Technical Paper 901242, 20th Intersociety Conference on Environmental Systems, Williamsburg, Virginia, July 9-12, 1990.
2. P. F. Dexter and W. L. Haskin, "Analysis of Heat Pump Augmented Systems for Spacecraft Thermal Control," AIAA Paper 84-1757, AIAA 19th Thermophysics Conference, Snowmass, Colorado, June 25-28, 1984.
3. B. Drolen, "Heat Pump Augmented Radiator for High Power Spacecraft Thermal Control," AIAA Paper 89-0077, 27th Aerospace Sciences Meeting, Reno, Nevada, January 9-12, 1989.
4. B. Penswick and I. Urieli, "Duplex Stirling Machines," SAE Paper 849045, 19th Intersociety Energy Conversion Engineering Conference, San Francisco, California, August 19-24, 1984.
5. F. C. Chen, E. G. Keshock, and R. W. Murphy, "Testing of a Stirling Cycle Cooler," *The Winter Annual Meeting of the American Society of Mechanical Engineers*, AES-Vol. 8, SED-Vol. 6, pp. 49-55, ASME, New York, 1988.
6. M. E. Ewert, P. P. Petete, and J. Dezenitis, "Active Thermal Control Systems for Lunar and Martian Exploration," SAE Paper 901243, *Advanced Environmental/Thermal Control and Life Support Systems*, Publ. SP-831, pp. 55-65, SAE, Warrendale, Pa., 1990.
7. G. A. Landis, S. G. Bailey, D. J. Brinker, and D. J. Flood, "Photovoltaic Power for a Lunar Base," *Acta Astronautica*, Vol. 22, pp. 197-203, 1990.
8. R. D. Waldron, "Lunar Base Power Requirements, Options, and Growth," *Engineering, Construction and Operations in Space 2; Proceedings of Space'90*, Part 2, pp. 1288-1297, 1990.

9. P. F. Dexter, R. J. Watts, and W. L. Haskin, "Vapor Cycle Compressors for Aerospace Vehicle Thermal Management," SAE Paper 901960, presented at the Aerospace Technology Conference and Exposition, Long Beach, California, October 1-4, 1990.

10. W. C. Reynolds, "Thermodynamic Properties in SI," Dept. Mech. Eng., Stanford Univ., Stanford, Calif., 1979.

11. H. Meitz and M. Gottmann, "FORTRAN77 Library to Compute Real Gas Properties," Univ. of Arizona, Tucson, 1992.

12. Carrier Air Conditioning Company, *System Design Manual*, Syracuse, New York, 1972.

13. *Engineering and Configurations of Space Stations and Platforms*, Noyes Publications, 1985.

14. L. Guerra, "A Commonality Assessment of Lunar Surface Habitation," *Engineering, Construction and Operations in Space; Proceedings of Space 88*, pp. 274-287, 1988.

15. M. Olszewski and U. Rockenfeller, "Heat Pump Augmented Radiator for Low-Temperature Space Applications,:

16. G. Grossman, "Heat Pump Systems for Enhancement of Heat Rejection from Spacecraft," *Journal of Propulsion*, Vol. 6, pp. 535-644, 1990.

17. E. J. Roschke and L. C. Wen, "Preliminary System Definition Study for Solar Thermal Dynamic Space Power Systems," Technical Report D-4286, JPL, Pasadena, California, 1987.

18. L. L. Begg and E. H. Engdahl, "Advanced Radiator Concepts," *Proceedings of the 24th Intersociety Energy Conversion Conference*, Washington, DC, August 6-11, 1989, pp. 75-80.

19. M. P. Moriarty and W. R. Determan, "SP-100 Advanced Radiator Designs for Thermoelectric and Stirling Applications," *Proceedings of the 24th Intersociety Energy Conversion Conference*, Washington, DC, August 6-11, 1989, pp. 1245-1250.

20. E. Trujillo, E. Keddy, and M. Merrigan, "Design and Demonstration of a High-Temperature, Deployable, Membrane Heat-Pipe Radiator Element," *Proceedings of the 24th Intersociety Energy Conversion Conference*, Washington, DC, August 6-11, 1989, pp. 1891-1895.

21. ASHRAE Handbook 1989 Fundamentals, ASHRAE, New York, 1989.